



Effect of twisted rib on the hydrothermal performance and entropy generation behavior in minichannel heat sinks cooled by biologically synthesized Ag/water nanofluid

Amin Shahsavari¹ · Mahan Hasani¹ · Çağatay Yıldız^{2,3} · Müslüm Arıcı^{2,3}

Received: 7 December 2023 / Accepted: 4 April 2024
© The Author(s) 2024

Abstract

This numerical research study focuses on impacts of using twisted rib geometry on the hydrothermal performance and entropy generation characteristics of biologically synthesized Ag/water nanofluid flowing in heat sink minichannels. To this end, twelve different twisted rib geometries (Case 1 to 12) were designed where the double-row ribs were twisted at the bottom and top portions with twist angles between -45° and $+45^\circ$. To elucidate the cooling performance comprehensively, four different Reynolds numbers ($Re = 500, 1000, 1500, \text{ and } 2000$) and four different nanoparticle concentrations ($\varphi = 0\%, 0.1\%, 0.5\%, \text{ and } 1\%$) were included in the numerical computations. Results revealed that using twisted ribs significantly smoothen the fluid flow and reduces pressure drop remarkably depending on twist angles, nevertheless, it deteriorates the cooling performance. In Case 12, the convective heat transfer coefficient reduces by up to 15.8% at $Re = 2000$ and $\varphi = 1\%$, compared to the base case. However, pumping power requirement is decreased by 43.9% in this case. Nanoparticle incorporation contributes to enhancement of convective heat transfer coefficient by up to 13.5% at the lowest Re . Frictional entropy generation considerably decreases (up to 31%) when twisted ribs are utilized. However, thermal entropy generation can increase up to 36%, due to ineffective cooling with twisted ribs. This work can be regarded as a first study in the field concerning the effects of top and bottom twist angles on hydrothermal performance and entropy generation in nanofluid-cooled mini-channel heat sinks.

Keywords Electronics cooling · Heat sink · Entropy generation · Biologically synthesized nanofluid · Twisted ribs · Twist angles

List of symbols

C_p	Specific heat ($\text{J kg}^{-1} \text{K}^{-1}$)
d_p	Particle diameter (m)
f_{drag}	Drag coefficient (-)
h	Convective heat transfer coefficient ($\text{W m}^{-2} \text{K}^{-1}$)
k	Thermal conductivity ($\text{W m}^{-1} \text{K}^{-1}$)
g	Gravitational acceleration (m s^{-2})
p	Pressure (Pa)
Re	Reynolds number

q''	Heat flux (W m^{-2})
S'''	Local entropy generation ($\text{W m}^{-3} \text{K}^{-1}$)
\dot{S}	Global entropy generation (W K^{-1})
T	Temperature (K)
u_x, u_y, u_z	Velocity component in Cartesian coordinates (m s^{-1})
V	Velocity (m s^{-1})
\dot{V}	Volume flow rate ($\text{m}^3 \text{s}^{-1}$)
V^*	Volume (m^3)
\dot{W}	Pumping power (W)
x, y, z	Distances in Cartesian coordinates (m)

✉ Müslüm Arıcı
muslumarici@gmail.com

¹ Department of Mechanical Engineering, Kermanshah University of Technology, Kermanshah, Iran

² Mechanical Engineering Department, Engineering Faculty, Kocaeli University, 41001 Kocaeli, Turkey

³ International Joint Laboratory on Low-Carbon and New-Energy Nexus Research and Development, Kocaeli University, 41001 Kocaeli, Turkey

Greek letters

φ	Nanoparticle volume fraction
μ	Dynamic viscosity (Pa s)
ρ	Density (kg m^{-3})
θ	Temperature uniformity index ($\text{m}^2 \text{K W}^{-1}$)

Subscripts

d	Drag
f	Fluid

fr	Frictional
n	Nanofluid
p	Nanoparticle
th	Thermal

Abbreviations

CHTC	Convective heat transfer coefficient
CPU	Central processing unit
EG	Entropy generation
FEG	Frictional entropy generation
<i>FoM</i>	Figure of merit
HTF	Heat transfer fluid
LVG	Longitudinal vortex generator
<i>PEC</i>	Performance evaluation criterion
TEG	Thermal entropy generation

Introduction

Remarkable downsizing of electronic components such as central processor units (CPUs) is attained within the rapid development of technologic devices in the last decades. Certainly, the act of miniaturization of these devices increases the heat flux passing through their body [1]. This phenomenon consequently increases the risk of damage related to excessive temperature rises, and research report that half of the failures in electronic components occurs due to excessive temperature rises [2]. Hence, a significant problem is arisen about thermal management of such devices, which challenges the researchers focusing on the improvement of reliability and lifespan of electronic components [3].

Overcoming of the issue of excessive temperature rise in electronic devices is mostly carried out by using heat sinks, which are simply successful in rejecting the dissipated heat from the surface of an electronic component [4, 5]. Heat sinks are usually made of highly conductive metals such as aluminum or copper, and they generally have extended surfaces to increase the heat transfer area outstandingly helping the heat rejection [6, 7]. Nevertheless, convective heat transfer around the heat sink and fins is of great importance to sufficiently remove heat from the component. Hence, air or a liquid can be used as a heat transfer fluid at this point. From this point of view, heat sinks can be mainly categorized into air or liquid cooling within the framework of natural or forced cooling [8], yet there may be additional techniques for heat transfer augmentation, which can be listed as fin addition with effective geometries [9], utilization of nanofluids [10, 11], consideration of improved channel geometry [12, 13], and using metal foams [14, 15]. It is noteworthy to mention that more than one technique can be implemented in an application to further acquire enhanced heat transfer [16, 17]. In addition to that, consideration of

boiling heat transfer is also investigated by researchers over the past couple of years [18].

Although air and liquid cooling methods in heat sinks have a common aim to thermally manage an electronic device, their effectiveness significantly varies from each other. As the heat capacity and thermal conductivity of liquids such as water are considerably higher than air, a large amount of heat transfer rate can be achieved using liquid-cooled systems [19, 20]. On the other hand, these systems usually require a more complex structure and are relatively expensive, while air-cooled heat sinks are simpler-structured and relatively inexpensive [21, 22]. For these reasons, selection of appropriate heat sink type may vary depending on various parameters and considerations. Yet, requirement of a large amount of heat removal brings the necessity of using liquid-cooled systems as expected. Nonetheless, conventional liquid-cooled systems operated via water or glycol circulation may be even insufficient in some applications [23]. At this point, a further enhancement of thermal properties in liquid-cooled heat sink systems may be demanded. Thermal conductivity enhancement of liquids circulating through the heat sink can significantly improve the heat removal rate, and this improvement can be accomplished by dispersing thermally high-conductive metallic nanomaterials in the base fluid. In this case, the resulting suspension is called nanofluid [24, 25]. In addition to that, using more than one type of nanoparticle inside the base fluid to improve the effectiveness and reduce some challenging phenomena, namely the consideration of hybrid nanofluids, has been recently popular for micro- and mini-channel heat sinks as well [26, 27]. Therefore, numerous recent works have focused on revealing the benefits of nanofluids in heat sinks under various operation conditions with different designs. In a recent study conducted by Ho et al. [28], a micro channel heat sink was investigated, and the use of water and alumina/water nanofluid is comparatively examined. The authors reported a significant decrement in the thermal resistance and a significant improvement in the convective heat transfer coefficient (CHTC), which were quantitatively indicated as 12.61% and 14.43%, respectively. Another lately done study [29] compared the thermal performance of CuO/water and Al₂O₃/water nanofluids by referencing the pure water. The experimental outcomes signified a remarkable thermal performance improvement using nanofluids instead of pure water. Furthermore, CuO/water nanofluid was found to be superior compared to alumina/water nanofluid for the cooling of electronic component, where the maximum enhancement in the average Nusselt number (Nu) was computed as 12.5% and 16.01% for Al₂O₃/water and CuO/water nanofluids, respectively, at $\phi=0.1\%$. It should be noted here that although the benefits of using nanofluids are emphasized in these studies, the considered heat sinks have various designs of fins as well. This means that heat sinks

are usually considered with fins, along with other thermal performance enhancers. As another instance using different thermal performance enhancers, Boudraa and Bessaïh [30] numerically considered a finned heat sink filled with aluminum foam, which has a liquid-cooled system using alumina-copper/water hybrid nanofluid as coolant. They indicated that heat transfer rate can be augmented by up to 72% and 40% adjusting the appropriate Darcy number and porosity values. Besides, using nanoparticles with a diameter of 20 nm attained 7% higher improvement in heat transfer, compared to 60 nm particles. Marseglia et al. [31] compared different strategies for heat transfer augmentation in microchannel heat sinks, and they reported that low concentration of Au, Ag, or Al₂O₃ nanoparticles, i.e., $\varphi < 1\%$, considerably help improving heat transfer. Similarly, Ma et al. [32] investigated the impact of Ag, SiO₂, and Al₂O₃ nanoparticles on the cooling performance of a microchannel heat sink, and they noted an improvement of average convective heat transfer coefficient up to 12.3%. They also optimized the particle volume fraction. Mukherjee et al. [33] focused on thermal performance and entropy generation characteristic in a microchannel heat sink cooled by nanofluids. The authors tested the impact of different nanofluids and concluded that utilization of nanofluids attain an augmentation of up to 24.95% in heat transfer, while it reduces the total entropy generation by 19.96%. Ho et al. [34] focused on the single and mini- and microchannel stacked double layer channel geometry of heat sinks cooled by nanofluids. Regarding the examination on the geometry of heat sink, the authors recommended the stacked double layer heat sink for enhanced cooling capability. Yan et al. [35] studied the effect of alumina and silica based nanofluids on the hydrothermal performance of a microchannel heat sink, which has a fractal channel structure by different levels. They found that the alumina water can enhance the convective heat transfer coefficient by 4% to 8.3%, while the pressure drop is increased by 28.58% to 32.09%, depending on the initial velocities.

Even though the nanoparticles and metal foams can effectively improve the energy transfer from the surface of electronic component to the cooler ambient, fins are indispensable key components of a heat sink in electronic industry, which can be also justified from numerous literature studies involving heat sinks together with fins [36–38]. Besides, fins in heat sinks not only improve heat conduction due to being made of thermally conductive materials and having extended surface area, but also they can significantly alter the fluid flow passing around them [39, 40]. Hence, fins have a double-sided effect in heat sinks where their overall impact should be attentively evaluated, instead of evaluating them only for heat conduction augmentation. For this purpose, researchers working in the field make significant effort to reveal the most beneficial fin designs to enhance heat transfer preserving the balance between the conduction

improvement and pressure drop. Fin shapes are crucial for these designs, and a relevant study conducted by Yan et al. [41] proposed a novel fin shape and numerically tested different arrangements to improve heat transfer. As a result, the average Nusselt number was improved by up to 30%, while attaining pressure drop via fin design. Lately, Azadi et al. [42] investigated four different shapes of mini pin-fins, namely square, trapezoidal, triangular and sinusoidal, in a heat sink regarding their entropy generation behavior. They stated that the lowest entropy generation was observed for sinusoidal fins, which is 66.23% lower than the heat sink with smooth channels taken as reference case. A resembling study conducted by Khetib et al. [43] where different nanoparticle and pin-fin shapes were considered. Regarding the outcomes of the study, the authors recommended using circular fins with brick-shaped nanoparticles to obtain the highest cooling performance among the investigated cases. The angle of fins along with the fin geometry is also an important parameter in heat sinks, and some novel fin designs are investigated in the literature by various researchers to further achieve an enhancement, such as oriented square shapes [44] and airfoil shape [45], considering the aim of attaining less pressure drop and higher cooling performance, which is achieved as reported. Such specific designs are generally used for altering the fluid flow, which enhances convective heat transfer inside the heat sink. Related to that, Zheng et al. [46] recently explored the cooling effectiveness of longitudinal vortex generators (LVG) in mini-channel heat sinks, which is another technique for heat transfer enhancement by using the flow-altering feature of such fins, as mentioned in the previous paragraph. Consequently, the authors brought a suggestion about the designed LVG after investigating the geometrical parameters. They pointed out the trapezoidal cross sections of the LVG for a superior heat transfer over rectangular cross sections. Furthermore, the authors presented the highly effective optimal geometrical parameters of the LVG, which yields a larger performance evaluation criterion (*PEC*). Focusing on channel geometry, Wang and Chen [47] investigated the effects of Koch fractal structure and nanofluid utilization on the thermal performance of a heat sink. The authors recommended the staggered baffle distribution inside the microchannel for a superior heat transfer, compared to other investigated distributions. Furthermore, the authors emphasized that increasing nanoparticle concentration is beneficial only up to a certain point. Li et al. [48] studied the hydrothermal performance of a microchannel heat sink having ribs and pin-fins. They used straight rectangular ribs where the rectangular cross-section fins are located between the ribs. The authors put an emphasis on the height of the ribs and pin-fins in order to improve heat transfer performance.

Effects of LVGs in heat sinks are studied in various research works considering different points of views. At this

point, Zhang et al. [49] explored that the length and number of LVGs have a significant role in improvement of Nu and overall efficiency, compared to other examined parameters, and these two quantities can be augmented up to 23.6% and 7.2%, compared to the reference case with original heat sink, according to the findings of the study. In a similar work, Zhang et al. [50] explored the impacts of twisting the ribs in the minichannels of a heat sink, and the researchers considered different twist angles ranging from 0 to 45° for the top and bottom of the ribs, while they additionally investigated the effect of their heights. The authors reported in this study that the highest cooling performance is achieved by using a rib having 0° top angle, 45° bottom angle along with 0.5 mm rib height, and they pointed out that twisted structures have a great potential for improving overall performance of mini-channel heat sinks.

Twisted rib or fin geometries were also found to be beneficial for heat sinks of electronic components in some experimental works of other research groups [51, 52]. Despite clearly having potential advantages for controlling the fluid flow and heat transfer inside the mini-channel heat sinks, the utilization of twisted ribs has been included in few studies in the literature. More importantly, the existing studies focusing on twisted ribs consider these geometries as a one row inside the channel, while they were considered to be dual parts in two different rows inside the mini channel within the scope of the present work. Furthermore, this study contributes to the existing literature by investigating the entropy generation characteristics when using double row twisted ribs, which are twisted both from bottom and top sections at different angles. In addition to that, elaboration the effects of using a biologically synthesized nanofluid on the fluid flow and heat transfer has not yet been investigated by the researchers, and it is foreseen that this would bring up another novel contribution to the field. At this point, in the present numerical study, different values for the bottom twisted angle (α) and top twisted angle (β) are considered

for both rows separately. Moreover, the effect of volume concentration of nanofluid ($\varphi=0, 0.1\%, 0.5\%$, and 1%) and Reynolds number ($Re=500, 1000, 1500$, and 2000) on the results has been investigated. As the present work presents a comprehensive insight into the hydrothermal performance and EG characteristics of twisted rib mini-channel heat sinks, it is hoped that the outcomes can be guidance for the researchers and engineers conducting studies in the field.

The paper continues thereafter with a detailed description of the problem and its mathematical modeling. Afterwards, the numerical procedure for the solution of the problem is presented together with the experimental verification of the numerical method. Then, the results are presented and discussed for hydrothermal performance and entropy generation, which are considered under two different subsections. Lastly, the conclusions drawn from the work are critically presented.

Problem description and mathematical modeling

The schematic views and dimensions of the considered mini-channel geometry for the heat sink can be found in Ref. [46] and are shown in Fig. 1. The ribs in the channel are twisted with different angles maintaining the length and width of the ribs as 1 mm and 0.2 mm, respectively, as per the twisted rib definition presented in [50]. Thereby, regarding this twisted rib definition for the presented mini-channel geometry with double-row ribs, there are 12 different combinations of heat sink channel with twisted ribs investigated, whereas plus-one case is included as the reference case where the ribs are not twisted. The front views of these twisted combinations along with the reference case are shown in Fig. 2. The bottom twist angles of the dual ribs (α_1 and α_2) and top twist angles (β_1 and β_2) corresponding to the designed 12

Fig. 1 Schematic representations of **a** isometric view of mini-channel geometry, **b** sectional side-view, **c** top-view and **d** single LVG [46] are given in order to illustrate the investigated twisted rib geometries inside the minichannel heat sink

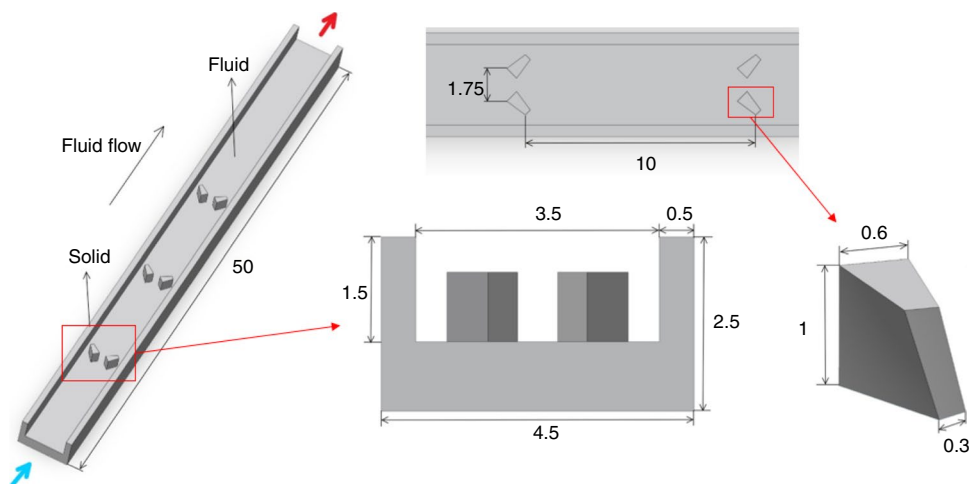


Fig. 2 Front views of the all considered twisted rib cases together with the twist angle values for each rib are shown. The base case includes the non-twisted ribs inside the minichannel, while the ribs are twisted from top and/or bottom sections by various angles in all other cases

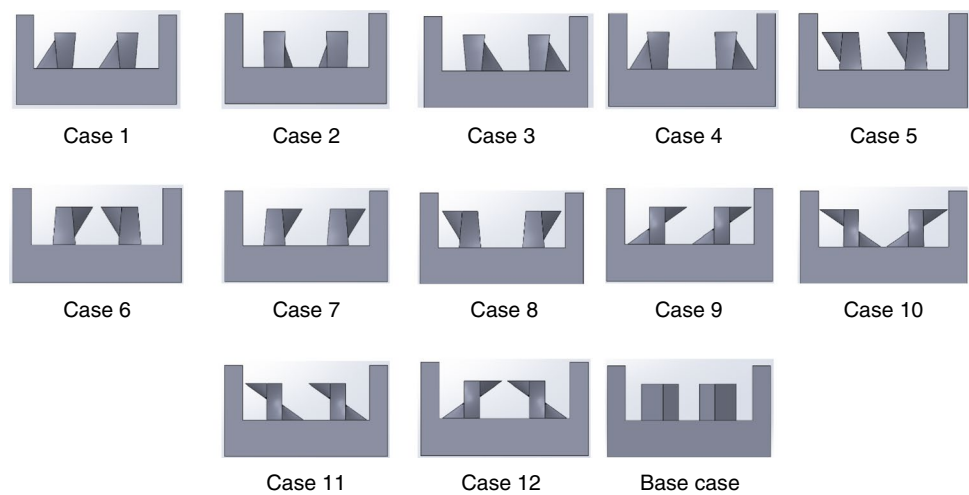


Table 1 List of bottom and top twist angles of the dual ribs located inside the mini-channel corresponding to designed cases

Cases	Bottom twist angle of rib 1 / α_1	Top twist angle of rib 1 / β_1	Bottom twist angle of rib 2 / α_2	Top twist angle of rib 2 / β_2
Case 1	45°	0°	45°	0°
Case 2	-45°	0°	45°	0°
Case 3	-45°	0°	-45°	0°
Case 4	45°	0°	-45°	0°
Case 5	0°	45°	0°	45°
Case 6	0°	-45°	0°	45°
Case 7	0°	-45°	0°	-45°
Case 8	0°	45°	0°	-45°
Case 9	45°	-45°	45°	-45°
Case 10	-45°	45°	45°	-45°
Case 11	-45°	45°	-45°	45°
Case 12	45°	-45°	-45°	45°
Base case	0°	0°	0°	0°

Cases for twisted ribbed mini-channel heat sink are shown in Table 1.

The coolant circulating through the heat sink channels is assumed to be Newtonian and incompressible, while the flow is considered laminar and steady. Biologically synthesized silver/water nanofluid is considered as coolant in the present work where the thermophysical properties of the base fluid and nanoparticles are given in Table 2 [53]. It is worth noting here that although there are various types of nanoparticles with different advantages such as the cost-effective ZnO particles [54], the Ag nanoparticles have a remarkably higher thermal conductivity that can boost up heat transfer significantly. Furthermore, the Ag nanoparticles considered in the present work are produced via an environment- and eco-friendly production process where the green tea leaf extracts are utilized, which is a biological and natural material used during the nanoparticle synthesis process.

Table 2 Thermophysical properties of solid nanoparticles and base fluid are given. The solid nanoparticles are biologically synthesized via a green method

Property	Ag	Water
Density/kg m ⁻³	10,500	997.1
Viscosity/kg m ⁻¹ s ⁻¹	-	0.001003
Specific heat capacity/J kg ⁻¹ K ⁻¹	235	4179
Thermal conductivity/W m ⁻¹ K ⁻¹	429	0.613

The mathematical model for the solution of parametric investigation of interest involves continuity, momentum, and energy equations along with the consideration of two-phase mixture model. Therefore, the aforementioned equations under the consideration of steady-state laminar flow, where the frictional losses and the radiative heat

transfer are neglected, can be respectively given as follows [55–57]:

$$\nabla \cdot (\rho_n V_n) = 0 \quad (1)$$

$$\nabla \cdot (\rho_n V_n V_n) = -\nabla p_n + \nabla \cdot (\mu_n \nabla V_n) + \nabla \cdot (\varphi \rho_p V_{d,p} V_{d,p} + (1 - \varphi) \rho_f V_{d,f} V_{d,f}) \quad (2)$$

$$\nabla \cdot [(\varphi V_p C_{p,p} + (1 - \varphi) V_f C_{p,f}) T] = \nabla \cdot (k \nabla T) \quad (3)$$

$$\nabla \cdot (\varphi \rho_p V_n) = -\nabla \cdot (\varphi \rho_p V_p) \quad (4)$$

The symbols p , T , and V indicate the pressure, temperature, and mass-average velocity, respectively, whereas the subscripts n, p, f, and d respectively stand for nanofluid, nanoparticle, base fluid, and drift. Nanoparticle volume fraction, density, and viscosity are signified by φ , ρ , and μ , while specific heat and thermal conductivity are symbolized by C_p and k , respectively. The mass-average velocity and drift velocity of the nanoparticles can be expressed as follows [55, 58]:

$$V_n = \sum_{k=1}^n \varphi_k \rho_k V_k / \rho_n \quad (5)$$

$$V_{d,k} = V_{pf} - \sum_{k=1}^n \varphi_k \rho_k V_{f,k} / \rho_n \quad (6)$$

In the above equation, V_{pf} signifies the relative velocity between a particle and the main fluid, and it is calculated as follows [59, 60]:

$$V_{pf} = \frac{\rho_p d_p^2 (\rho_p - \rho_n)}{18 \mu_f \rho_p f_{drag}} (g - (V_n \nabla) V_n) = V_p - V_f \quad (7)$$

In the equation giving the relative velocity, the gravitational acceleration, diameter of the nanoparticle, and the drag coefficient are respectively denoted by g , d_p , and f_{drag} . The drag coefficient is given by the equations as follows [61, 62]:

$$f_{drag} = \begin{cases} 1 + 0.15 \text{Re}_p^{0.687} & \rightarrow \text{Re} \leq 1000 \\ 1 + 0.15 \text{Re}_p & \rightarrow \text{Re} > 1000 \end{cases} \quad (8)$$

The boundary conditions required for the solution of the above-mentioned governing equations of the problem involves a constant temperature at the inlet section, which is considered 293 K, while the coolant is assumed to be discharged to the atmosphere. A heat flux value of $q'' = 100 \text{ kW m}^{-2}$ is imposed constantly to the bottom surface of the heat sink, and all the remaining walls as well as the top cover are considered as perfectly insulated. The

velocity and temperature profiles at the inlet section are uniform, and no-slip boundary condition is considered at the internal walls.

The thermophysical properties of the utilized nanofluid are estimated by various correlations involving the particle volume fraction along with the properties of the base fluid and the nanoparticles. The density and specific heat of the nanofluid are determined regarding the well-known mixture rule, which is expressed as follows [63]:

$$\rho_n = (1 - \varphi) \rho_f + \varphi \rho_p \quad (9)$$

$$C_{p,n} = [(1 - \varphi) \rho_f C_{p,f} + \varphi \rho_p C_{p,p}] / \rho_n \quad (10)$$

The dynamic viscosity and thermal conductivity of the Ag/water nanofluid are obtained using following equations, where the thermal conductivity of the coolant is considered to be dependent on the temperature, (T in Celsius) [64].

$$\mu_n = (1 + 2.5\varphi) \mu_f \quad (11)$$

$$k_n = k_f [0.00114T + 30.661\varphi + 0.981] \quad (12)$$

Several performance parameters are defined within the framework of the present study in order to accurately evaluate the hydrothermal performance and EG characteristics of the nanofluid flowing through the twisted rib heat sink. The highest temperature reached on the CPU is an important parameter that measures the degree of cooling. In addition to that, CHTC denoted by h , and the index of temperature uniformity (θ) are significant indicators for the determination of the level of convective heat transfer and the uniformity of temperature distribution on the CPU, respectively. These are defined by the following expressions [59]:

$$h = \frac{q''}{T_{\text{CPU,mean}} - T_m} \quad (13)$$

$$\theta = \frac{T_{\text{CPU,max}} - T_{\text{CPU,min}}}{q''} \quad (14)$$

Here, the subscripts of the temperature values, max, min, and mean respectively stand for the maximum, minimum, and mean temperature values on the CPU, while T_m indicates the arithmetical average of the fluid temperature of the inlet and outlet. Also, it should be stressed out that a lower θ indicates a more uniform temperature distribution on the CPU where the possibility of hot-spot phenomenon is lower.

Apart from cooling performance, pumping power is a crucial performance parameter as well, due to the fact that using nanofluids are likely to alter the pressure drop as the dynamic viscosity and density considerably change by the addition of solid nanoparticles into a base fluid. Therefore,

pumping power required to circulate the nanofluid through heat sink is evaluated within the present work as given below [65, 66]:

$$\dot{W} = \dot{V}\Delta p \quad (15)$$

In the given equation, \dot{W} , \dot{V} , and Δp respectively denote the pumping power, volumetric flow rate, and the pressure drop. A holistic determination of heat transfer performance along with pressure drop characteristics to fully understand the hydrothermal performance from these two points of view is needed to obtain a reasonable assessment. Thus, the *PEC* is defined as follows, which indicate the relative augmentations in both CHTC and pressure drop in the examined twisted rib cases, compared to the base case [67, 68]:

$$PEC = \frac{h_{\text{Case-n}}/h_{\text{Basecase}}}{(\Delta p_{\text{Case-n}}/\Delta p_{\text{Basecase}})^{1/3}} \quad (16)$$

A similar relation is established to assess the benefits of nanofluid utilization, which is the figure of merit (*FoM*), and it is defined as follows [69, 70]:

$$FoM = \frac{h_n/h_f}{(\Delta p_n/\Delta p_f)^{1/3}} \quad (17)$$

The performance evaluation of the twisted rib heat sink is conducted regarding both first and second laws of the thermodynamics. Hence, the EG within the coolant is investigated for all considered cases. The EG can be divided into two branches here: (i) frictional entropy generation (FEG) mainly occurred due to the fluid flow intensity and pressure drop inside the heat sink, and (ii) thermal entropy generation (TEG) arisen because of the variations in the temperature gradient i.e., conductive and convective heat transfer. These two types of EGs, namely FEG and TEG, can be locally expressed per unit volume, as respectively given below [71, 72]:

$$S_{\text{fr}}''' = \frac{\mu_n}{T} \left\{ \left[\left(\frac{\partial u_x}{\partial x} \right)^2 + \left(\frac{\partial u_y}{\partial y} \right)^2 + \left(\frac{\partial u_z}{\partial z} \right)^2 \right] + \left(\frac{\partial u_x}{\partial y} + \frac{\partial u_y}{\partial x} \right)^2 + \left(\frac{\partial u_x}{\partial z} + \frac{\partial u_z}{\partial x} \right)^2 + \left(\frac{\partial u_y}{\partial z} + \frac{\partial u_z}{\partial y} \right)^2 \right\} \quad (18)$$

$$S_{\text{th}}''' = \frac{k_n}{T^2} \left[\left(\frac{\partial T}{\partial x} \right)^2 + \left(\frac{\partial T}{\partial y} \right)^2 + \left(\frac{\partial T}{\partial z} \right)^2 \right] \quad (19)$$

$$S_{\text{total}}''' = S_{\text{fr}}''' + S_{\text{th}}''' \quad (20)$$

In the above equations, the subscripts fr and th stand for the frictional and thermal. The velocity components in the x , y , and z directions in the Cartesian coordinates are given by u_x , u_y , and u_z .

The global entropy generation values for frictional and thermal parts can be obtained by integrating the local values over the entire domain volume (V^*), and this can be mathematically expressed as follows:

$$\dot{S}_{\text{fr}} = \int S_{\text{fr}}''' dV^*; \dot{S}_{\text{th}} = \int S_{\text{th}}''' dV^*; \dot{S}_{\text{total}} = \int S_{\text{total}}''' dV^* \quad (21)$$

Numerical implementation

The three-dimensional steady-state problem in consideration is handled with a finite-volume based commercial CFD solver ANSYS Fluent 18.1, where the pressure–velocity coupling is implemented by SIMPLE algorithm. Discretization of the convective terms are carried out by second-order upwind scheme, and the convergence criteria is set to 10^{-6} for the solution of all considered governing equations within the problem.

In order to assure the solution is not dependent on the grid, five grids with different numbers of elements were prepared for Case 12 and the $T_{\text{CPU,max}}$ and Δp were determined at $\varphi = 1\%$ and $\text{Re} = 2000$ by using them. Regarding the outcomes of the study given in Table 3, it was found that increasing the number of elements to more than 4,467,209 has a negligible effect on the results, and as a result, the grid with 4,467,209 elements was chosen to perform the required simulations.

Ensuring the validity of the results is of utmost importance for numerical studies. Therefore, the experimental study of Liu et al. [73] in the literature was considered for verification of the present numerical procedure. In the considered experimental work [73], hydrothermal performance of silicon-made rectangular microchannel with five pairs of LVGs is taken into account, where the coolant is pure water. For the experimental verification of the current numerical implementation, the dimensions and boundary conditions reported in Ref. [73] were considered for the microchannel, and the thermophysical

Table 3 Results of the grid independence test are presented, and it is observed from the set of simulations that increasing the number of elements beyond 4,467,209 has insignificant effect on the results which ensures that the solution is independent from the grid when the number of elements is considered 4,467,209

Number of elements	$T_{\text{CPU,max}}/\text{K}$	$\Delta p/\text{Pa}$
1,163,365	305.496	1943.548
2,439,901	303.902	1877.001
3,476,003	302.567	1811.43
4,467,209	301.478	1761.964
5,203,654	301.355	1758.779

properties mentioned in Ref. [74] for silicone were taken into account. The microchannel performance investigated in Ref. [73] was simulated by applying the numerical method described in this research. The results obtained from two studies for the average Nusselt number at different Re values are shown in Fig. 3. The maximum difference between the findings of the two studies is less than 11.9%, and this difference can be attributed to the experimental laboratory conditions and circumstances in the experimental work, which cannot be fully compensated by numerical works. Furthermore, it was also indicated in the experimental work considered for the validation study that the uncertainty in Nusselt number increased by increasing Reynolds number. Hence, considering the experimental nature of the study performed in Ref. [73], the validity of the numerical model is regarded to be acceptable.

Results and discussion

This work explores the effect of twisted ribs with different top and bottom twist angles on the hydrothermal performance and EG behavior of the nanofluid-cooled heat sink. The considered nanofluid has biologically synthesized Ag nanoparticles, which makes it an environment-friendly product. The study involves four different Reynolds numbers ($Re = 500, 1000, 1500,$ and 2000) and four different nanoparticle volume fractions including the base fluid ($\varphi = 0\%, 0.1\%, 0.5\%$, and 1%), along with 12 different cases of twisted ribs and one base case as reference. The discussion of the

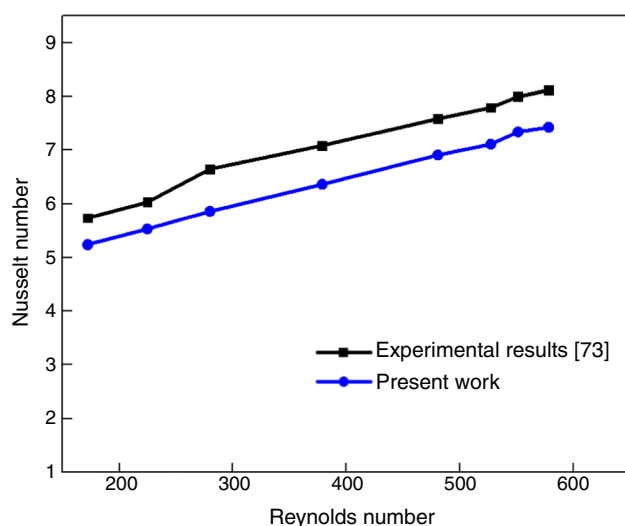


Fig. 3 Comparison of the results for the model validation is given, and the discrepancy between the present results and the experimental results in the relevant literature is less than 11.9% which assures the credibility of the present numerical solution, considering the experimental conditions of the study presented

results are handled in two different subsections, namely hydrothermal performance and entropy generation characteristics. The outcomes for hydrothermal performance are discussed over velocity and temperature contours, and the predefined performance parameters such as CHTC, maximum temperature, temperature uniformity index, *PEC*, and *FoM*. Under the second subsection, the entropy generation characteristics are discussed over contours illustrating local FEG and TEG values and the figures displaying their global values. It is expected that the discussion of the results provide an insight to the effects of twisted ribs on the aforementioned phenomena.

Hydrothermal performance

The basic understanding of the flow structure of the heat transfer fluid including nanoparticles which circulates in the minichannels can be well attained by the examination of velocity contours along with vectors. Figure 4 depicts the velocity contours together with the vector illustration for all investigated cases at $Re = 2000$ and $\varphi = 1\%$. It is clearly noticed from these contours that the nanofluid has a relatively higher flow resistance in the base case, where no twisted geometry is considered, compared to the other cases which include twisted ribs. Furthermore, it is also noticed that the nanofluid flow becomes smoother examining the contours from Case 1 through Case 12. This means that, especially when the considered ribs are twisted from both top and bottom parts, the flow turns out to be smoother while passing around the twisted ribs inside the mini-channel. This is because of the relatively lower viscous effects caused by the friction factor in twisted rib cases, compared to the reference case where the rib body is bluff and leads to a higher friction factor. This impact is more profound when the ribs are twisted at both top and bottom due to the fact that the bluntness of the rib geometry is thereby decreased, hence, it leads to a lower effect on velocity boundary layer and a reduction in pressure drop. In consistency with this interpretation, it is noted that the nanofluid velocity is noticeably higher while passing around the ribs in base case, which indicates a Venturi effect between the bluff body ribs. On the other hand, especially in Cases 2, 10 and 12, the fluid velocity is relatively lower compared to other cases, pointing out a smoother transition of the nanofluid through these twisted ribs. More insight can be given by the velocity contours of the base case as well as Case 2, 10, and 12, which are marked by the red dashed frame focusing on the twisted rib geometries. As seen from the figure indicating these particular areas, the fluid velocity is noticeably low in front of the ribs of the base case. This shows that the untwisted rib geometry in the base case constitutes a barrier for the upstream, which causes a significant flow resistance. In addition to that, this phenomenon causes a relatively larger low-velocity zone

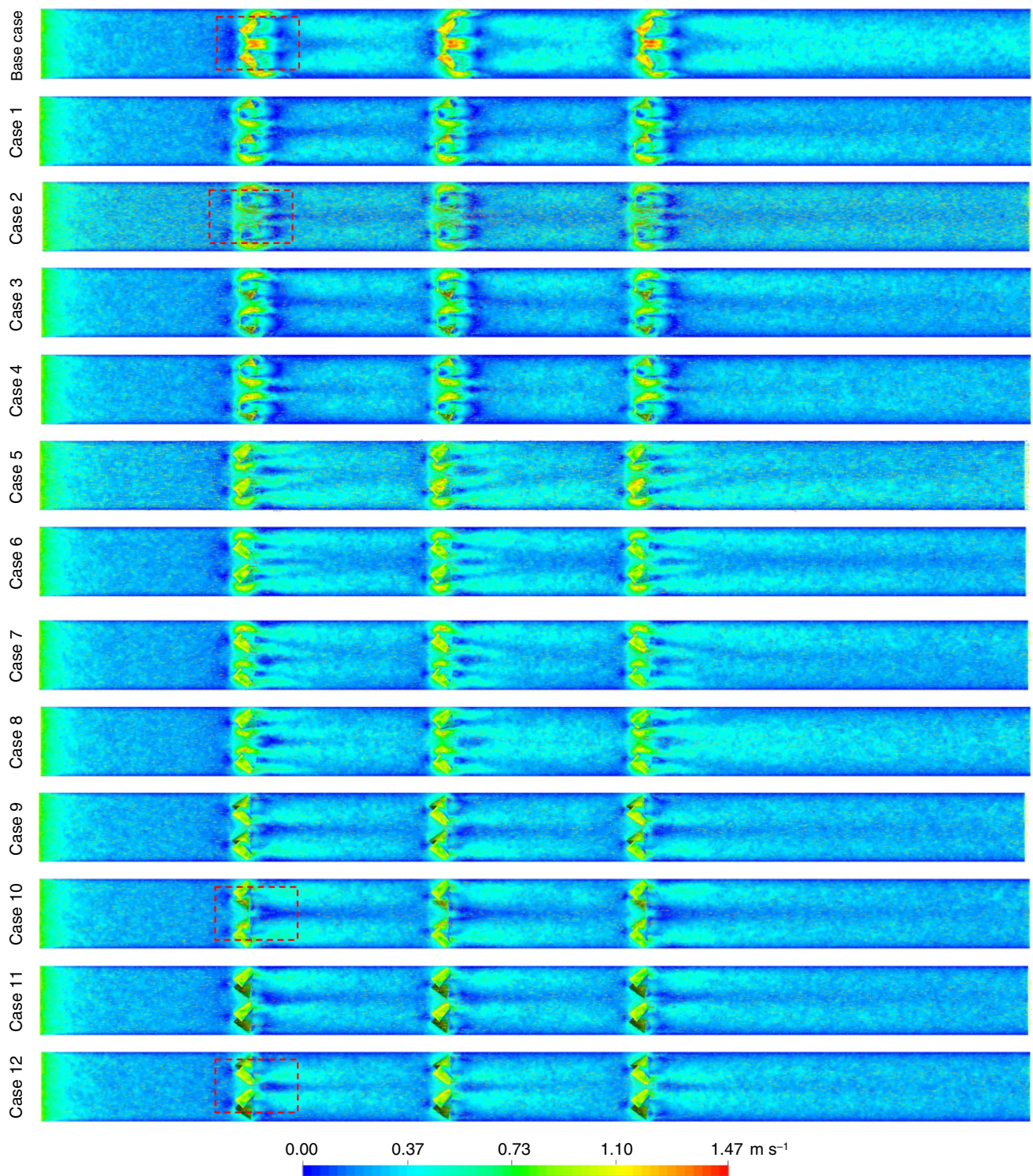
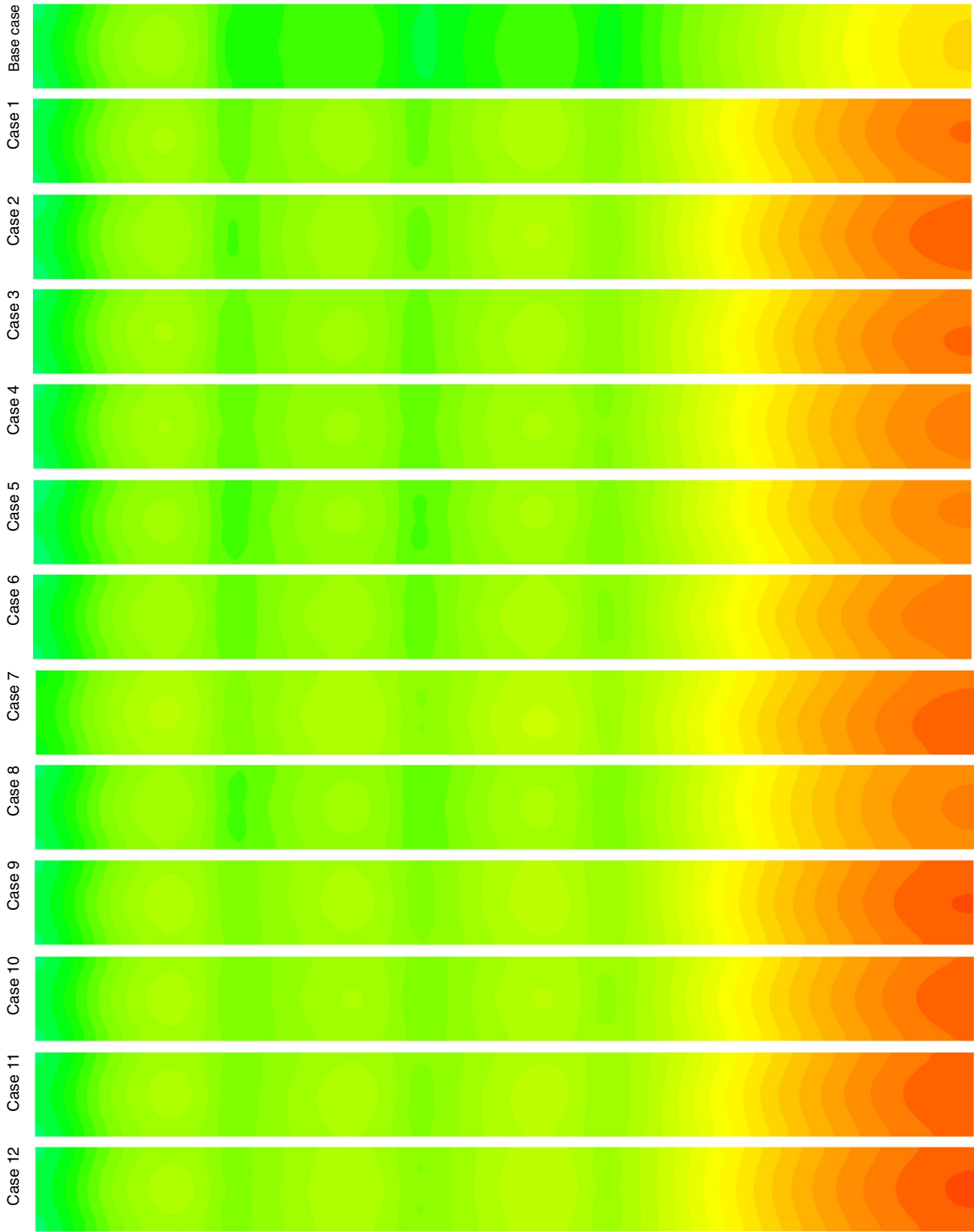


Fig. 4 Velocity contours are given inside the heat sink for the base case and the Cases 1 to 12 at $\phi=1\%$ and $Re=2000$. It is observed that the flow velocity around the nontwisted ribs in the base case is

downstream of the flow behind the ribs, meaning that there is a backflow which may deteriorate the flow structure and convective motions. On the other hand, the resistance is

relatively higher compared to other cases due to the narrowing flow path through the ribs, while twisting the ribs from bottom and top attains a smoother fluid flow around the ribs

lower in front of the twisted ribs, particularly given in Case 2, 10, and 12, which is reflected to the contours with smaller low-velocity zones, both upstream and downstream of the



292.9 295.1 297.4 299.6 301.8 K

Fig. 5 Temperature profiles on the CPU surface are illustrated for the base case and the Cases 1 to 12 at $\varphi = 1\%$ and $Re = 2000$. It is clearly seen that the temperature is significantly high for the Cases 2, 10, and 12 together with hotspots. In the base case, the temperature values are lower indicating a higher rate of cooling compared to other cases having twisted ribs

flow. As evidently seen from the figure, the velocity values are larger behind the twisted ribs due to smoother fluid flow around the twisted ribs, which consequently help reducing pressure drop.

Considering the convective heat transfer inside a heat sink, such as the problem of interest within the present work, the fluid flow structure has a direct impact on the temperature distribution on the CPU, which is shown by isotherms given for $Re = 2000$ and $\varphi = 1\%$ in Fig. 5. Examining all the given contours for all cases holistically, the temperature on the heat sink is lower near the inlet section as well as the middle regions, whereas the temperature exhibits a significant increase through the outlet section. The reason is that the temperature gradient in the direction from the CPU surface to the nanofluid flow is high around the inlet region, which leads to a high heat transfer from the CPU surface. However, the temperature difference between the nanofluid and CPU surface decreases while the heat transfer fluid (HTF) flows towards the outlet section since the nanofluid rejects heat from the CPU surface, and its temperature increases because of this energy absorption. Thus, through the outlet section, the temperature gradient in the direction from CPU to nanofluid decreases, which consequently leads to a lower heat transfer. Therefore, the regions near the outlet section of the mini-channel are at higher temperatures. Yet, considerable differences between the temperature distributions in the examined cases are obviously seen from the contours because of the variation of flow structures caused by different twist angles of the ribs. Drawing attention by noticeably cooler CPU surface compared to other cases, the cooling performance of the nanofluid in the base case is remarkably high. On the other hand, significantly higher temperatures are observed in the regions near the outlet section of the Cases 1 to 12, and these high-temperature-regions are significantly larger compared to base case. In addition to that, some cases, such as Case 1, 2, 3, 9, and 12, exhibit notable hotspots on the CPU surface, which indicates an ineffective cooling. Also, it can be inferred that the cases which have ribs with twist angles smoothing the fluid flow yields higher temperatures or even hotspots on the CPU surface. The reason why this phenomenon occurs is the relatively unrestricted and freer flow of the nanofluid in the cases such as Case 2, 10, and 12, where the nanofluid does not make strong vortices and complex enough fluid structure that can boost up the convective currents. Hence, an easier passage of the nanofluid around the ribs decreases

the effectiveness of the heat transfer, i.e., the cooling rate from the CPU. Relatedly, it is evidently noticed from the contours that the regions around the highly twisted ribs (such as the aforementioned Cases 2, 10, and 12) are at a higher temperature, compared to the base case. On the other hand, a higher pressure drop may be expected in the cases, where the fluid flow is relatively more restricted, e.g., the base case. Therefore, a holistic examination is needed in such cases in order to fully understand and reveal the hydrothermal performance of the minichannel geometry. For this purpose, the heat transfer enhancement and pressure drop should be evaluated as a whole, and a performance evaluation criterion (PEC) was also defined within the present work to reveal the overall performance.

CHTC obtained by the computations are given with respect to variation of φ at different Reynolds numbers in Fig. 6. An overview to the line graphs shows that increasing nanoparticle volume fraction causes a remarkable enhancement in the CHTC for all investigated cases. Since the nanoparticles added into the base fluid enhances the effective thermal conductivity, the heat transfer capability of the HTF increases, which provides a higher rate of heat rejection. Furthermore, Brownian-motion effects are also an important parameter causing an enhancement in the CHTC. Besides, an obvious increase in the CHTC is seen with increasing Re , which is caused by increasing flow intensity leading to an intensification of convection currents. More interestingly, it is seen that the base case exhibits remarkably higher CHTC values compared to other 12 cases, where the ribs are twisted from top and/or bottom with angles ranging from -45° to 45° . This can be grounded upon the complex flow characteristic caused by the bluff structure of the ribs in the base case, which leads to more intensified convection currents, as previously discussed over velocity and temperature contours.

Quantitative evaluation of the nanoparticle effect can be expressed by the comparison of the results at $Re = 500$ and $Re = 2000$, as the lowest and highest considered Re , and for the base case and Case 12 which are seen to yield the highest and lowest CHTC values among the investigated cases. At $Re = 500$ in the base case, addition of the particles at a volumetric concentration of $\varphi = 0.1\%$, 0.5% , and 1% enhances CHTC by 1.4% , 7.0% , and 13.5% , respectively, compared to $\varphi = 0$. At $Re = 2000$, these augmentation rates regarding the same volume fractions are 1.3% , 6.2% , and 11.6% , respectively. Considering Case 12, the enhancement caused by the addition of nanoparticles is 1.4% , 6.7% , and 12.9% at $Re = 500$, and 1.2% , 5.6% , and 10.6% at $Re = 2000$, when the volume concentration is switched to $\varphi = 0.1\%$, 0.5% , and 1% , respectively. Although the enhancement rates in the base case and Case 12 are similar for the investigated Re , yet it is noticed that the augmentation is slightly higher in the base case, which is related to the flow characteristics allowing nanoparticles

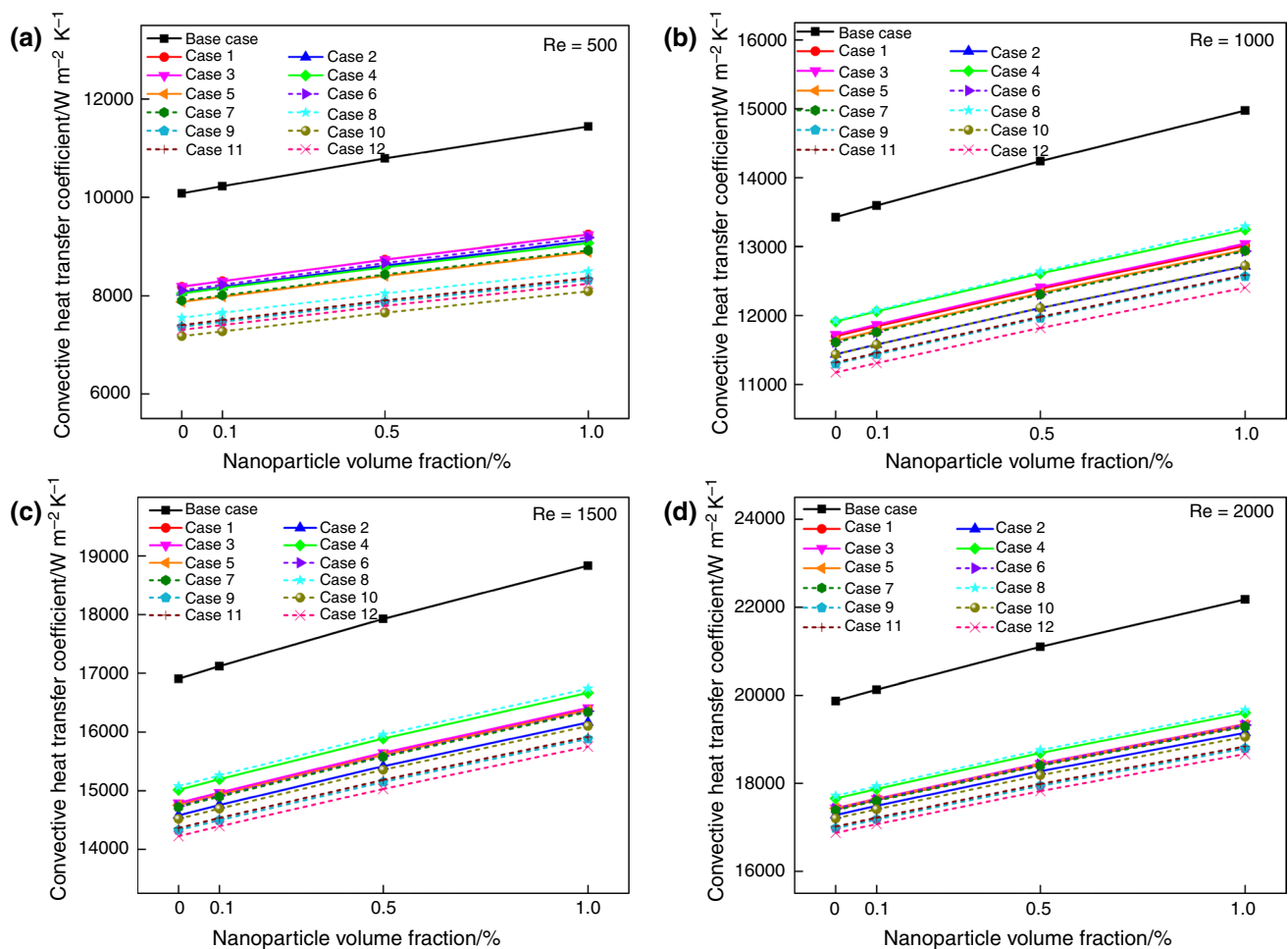


Fig. 6 CHTC values are given for all investigated cases with respect to variation of φ at **a** $Re=500$, **b** $Re=1000$, **c** $Re=1500$, and **d** $Re=2000$. For all Re , the CHTC is higher for the base case. Besides,

it significantly increases by increasing φ , which reaches up to 13.5% in the base case. In addition, Re has a direct impact on the CHTC, thus, its increase remarkably increases the CHTC values

to contribute more to the heat transfer by their complex motion inside the fluid as well as the Brownian effect. Furthermore, the impact of nanoparticles is relatively more dominant at low Re since they are more effective in conduction-dominant cases, as pointed out in various literature studies [75]. Besides, Case 12 is noted to have the lowest CHTC at $Re = 1000$, 1500, and 2000. Although it exhibits a slightly higher CHTC compared to other three cases at $Re = 500$, Case 12 can be regarded as the worst case from this point of view. In addition, Case 4 is seen to have a moderate CHTC as deduced from the figure. Thus, the base case, Case 4, and Case 12 can be selected for evaluating the performance of ribbed mini-channel heat sink at different twist angles of ribs. Thereby, to compare the CHTC among these selected cases at $Re = 2000$ and $\varphi = 1\%$, it was computed that the CHTC in Case 4 and Case 12 are respectively 11.6% and 15.8% lower,

compared to that in base case, due to the above-mentioned physical phenomena related to fluid flow.

Effect of CHTC variation regarding the flow structures and heat transfer characteristics depending on twisted rib geometries is reflected to the maximum temperature values on the CPU surface, which are shown in Fig. 7. In the previous discussion, the CHTC was found to be significantly higher in the base case compared to other cases; hence, the maximum temperature value observed on the CPU surface is notably lower in the base case, at all Re and φ values. Besides, Case 12 is noted to have the highest CPU temperature at $Re = 1000$, 1500, and 2000. For the same reason explained in the previous paragraph for CHTC, the base case, Case 4, and Case 12 can be selected for evaluating the cooling performance of ribbed mini-channel heat sink at different twist angles of ribs. At $Re = 2000$ and $\varphi = 1\%$, the maximum temperature of the CPU is respectively 0.99 K and 1.31 K higher in Case 4 and Case 12, compared to the base

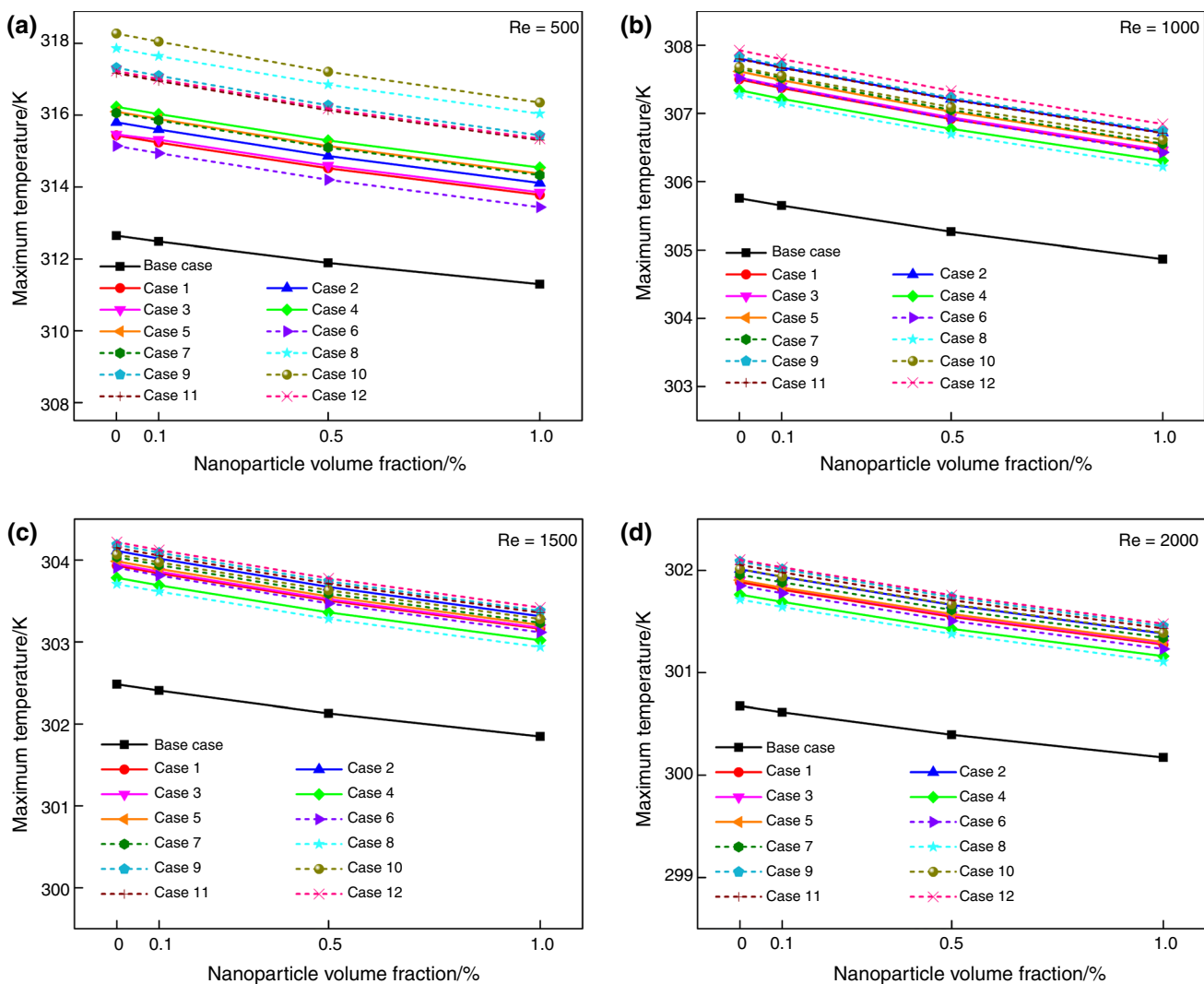


Fig. 7 Maximum temperature values are presented for all investigated cases with respect to variation of ϕ at **a** $Re = 500$, **b** $Re = 1000$, **c** $Re = 1500$, and **d** $Re = 2000$. Related to the increment in CHTC, a significantly larger cooling rate is ensured in the base case, and the maximum temperature values are obtained to be the lowest in the

case, which shows that the bluff structure of the ribs, i.e., no twisting effect, ensures a higher rate of cooling. Considering the quantitative effect of nanoparticle addition in the base case at $Re = 2000$, it was computed that inclusion of Ag particles at a concentration of $\phi = 0.1\%$, 0.5% , and 1% brings a reduction in the maximum temperature around 0.06 K, 0.28 K, and 0.50 K. Compared to nanoparticle enhancement, the numerical outcomes revealed that the effect of Re on the cooling performance is superior. For instance, in the base case at $\phi = 1\%$, when Re is progressively augmented from $Re = 500$ to $Re = 1000$, and then to $Re = 1500$, and lastly to $Re = 2000$, the reduction in the maximum temperature was calculated as 6.43 K, 3.02 K, and 1.67 K, respectively. On the other hand, the reduction effect of Re increment on the

base case. In the cases having twisted ribs from top and bottom, the reduction in the maximum CPU temperature is limited, due to the smoother fluid flow and its ineffectiveness in heat rejection. Besides, nanoparticle addition significantly helps reducing maximum temperatures on CPU surface, reaching up to 0.50 K

maximum temperature is more profound in Case 12, which was calculated to be 8.50 K, 3.42 K, and 1.94 K, for the same increment progression of Re . This is attributed to the flow structure in Case 12, which has likely lower pressure drop because of the shape of twisted ribs. Hence, increasing Re attains a more effective cooling because of higher inertial forces acting on the fluid, compared to viscous forces. Nevertheless, considering the overall outcomes, the base case with untwisted ribs ensures obviously a higher cooling performance due to exhibiting a more complex flow structure triggering the onset of convection currents.

Temperature uniformity is an important parameter for heat sinks. Even if the average temperature on the CPU could be in an acceptable range, hotspots may occur on the

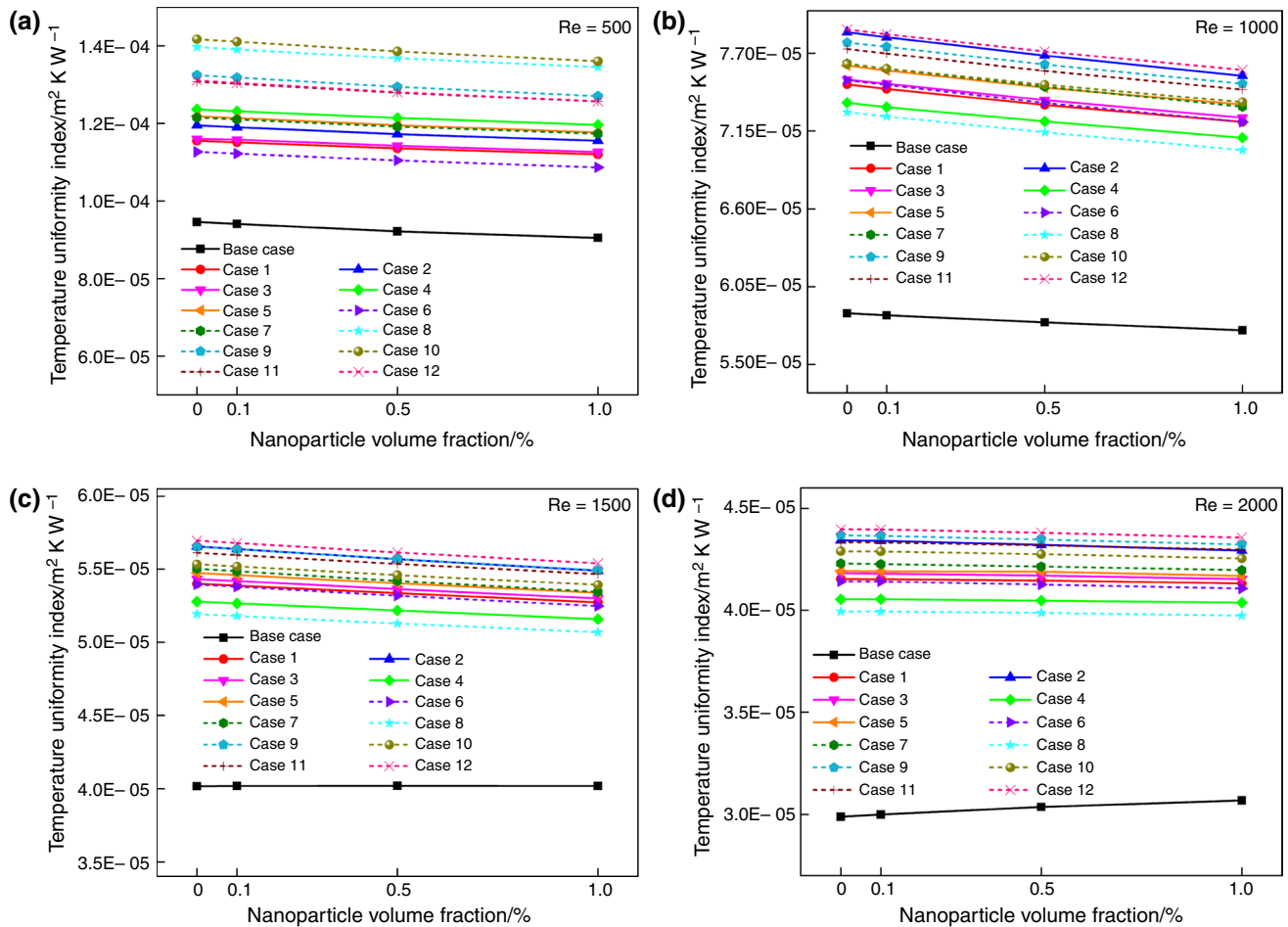


Fig. 8 Temperature uniformity index is presented for all investigated cases with respect to variation of ϕ at **a** $Re=500$, **b** $Re=1000$, **c** $Re=1500$, and **d** $Re=2000$. At $Re=500$, the temperature uniformity is significantly dependent on twist angles. Besides, temperature

uniformity index is the lowest for the base case indicating that the temperature is the most uniform in this case compared to other investigated ones

CPU which are hazardous for its operation since they can damage a certain portion or part of the CPU due to excessive local temperature rise. Therefore, the results of the temperature uniformity index defined in the previous section are given in Fig. 8. Similar to the previous discussions, the base case has the lowest temperature uniformity index, which means that the temperature distribution is the most uniform in this case, compared to other 12 cases. On the other hand, the cases having twisted ribs cannot ensure a temperature distribution as uniform as in the base case. Referring to the temperature contours given in Fig. 5, the cooling effect of the nanofluid on the CPU surface is higher at the inlet section of the mini-channel, and it decreases towards the outlet due to the heat rejection by nanofluid which decreases the temperature difference between the CPU surface and nanofluid. Nonetheless, in some cases, the temperature difference between the inlet and outlet sections is high, which causes a temperature non-uniformity along the mini-channel, and

thus, endangers the operation of CPU. The reason for this high temperature non-uniformity in cases such as Case 9, 10, or 12 is that the twisted ribs aid the fluid flow to be smoother without any significant impediment along the mini-channel. Thus, the HTF does not exhibit any vorticity or complex flow that help boosting the heat transfer. Hence, the HTF cannot effectively reject heat as it directly passes through the mini-channel, which causes an inefficient cooling and a larger temperature in the regions of CPU surface near the outlet. As another parameter investigated, increasing Reynolds number significantly decreases the temperature uniformity index, which means that a more uniform temperature distribution is obtained on the plane. As seen from the figure, the temperature uniformity index in the base case decreases roughly 70% when Reynolds number is increased from $Re=500$ to 2000. Besides, nanoparticle addition is also helpful for achieving temperature uniformity. However, its impact on this achievement decreases noticeably by increasing Reynolds number,

which is expected due to the fact that nanoparticles are more beneficial in conduction-dominant heat transfer, while their enhancement effect decreases when convective heat transfer dominates the situation.

Using a pump is a necessity to compensate the pressure drops occurring due to various reasons along the mini-channel. These pressure drops are sourced by several aspects such as the geometry of the twisted ribs in the mini-channel, level of Re , and the concentration of nanoparticles in the HTF. Therefore, pumping power requirement is shown in Fig. 9 for all the investigated cases. Unlike the cooling performance, the base case shows the worst hydraulic performance inside the mini-channel by requiring the highest pumping power, which is sourced by significantly higher pressure drop compared to other examined cases. The twisted

geometry of the ribs considerably decreases the pressure drop inside the mini-channel due to having lower friction factor caused by their curvy body rather than a bluff body structure. Hence, heat sinks having this type of twisted ribs require lower pumping power. Moreover, the cases having both ribs twisted at the top and bottom sections in opposite directions, i.e., Case 10 and Case 12, have the lowest pumping power requirement, since they constitute a smooth passage geometry for the fluid flow. Quantitative outcomes revealed that the pumping power required for the heat sink in Case 4 is lower by 28.1%, 31.4%, 33.8%, and 35.0% at $Re=500, 1000, 1500,$ and $2000,$ respectively, compared to the requirement in the base case. In Case 12, these reduction rates are more profound, and they are respectively 33.5%, 38.1%, 41.9%, and 43.9% lower at $Re=500, 1000, 1500,$ and

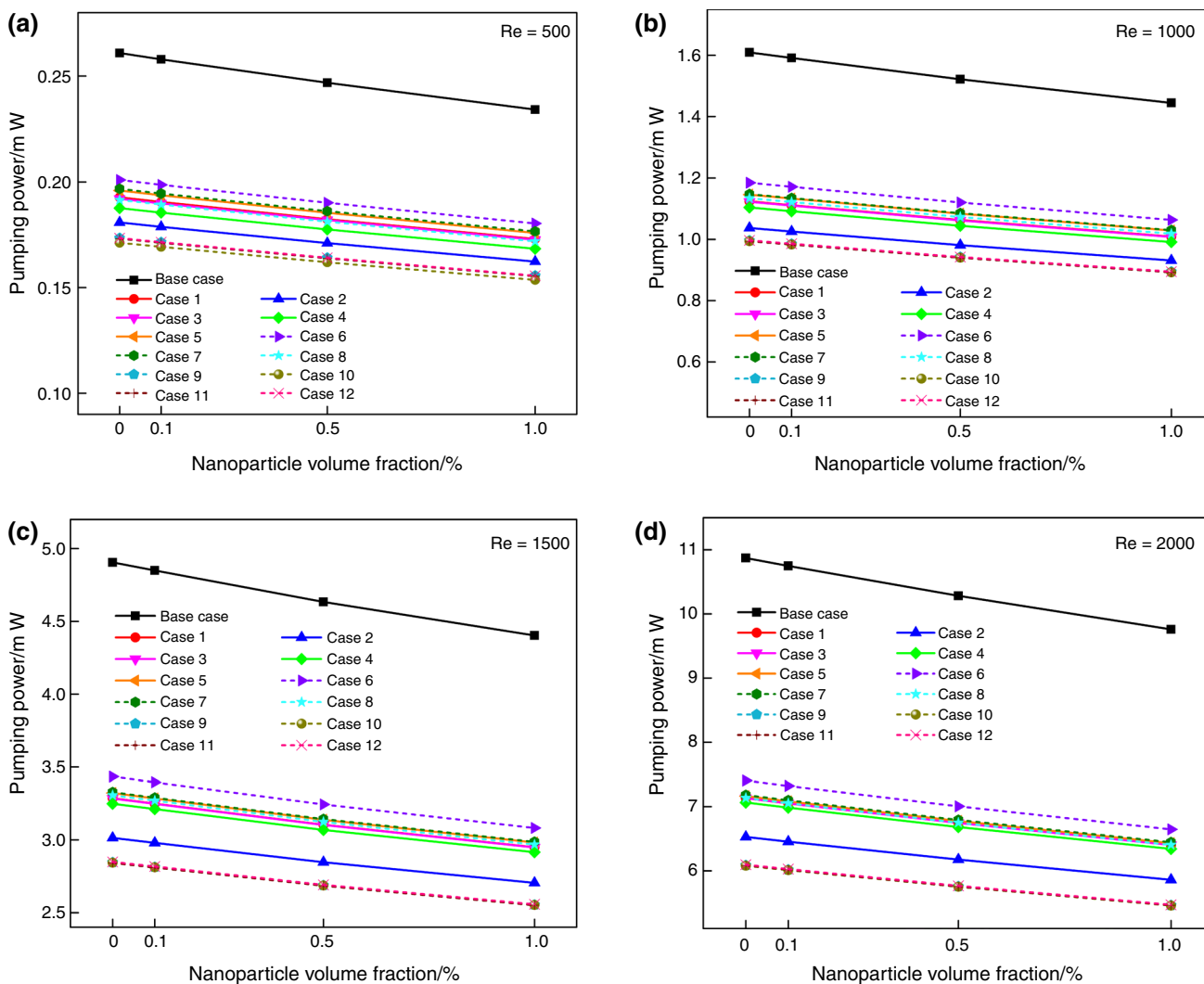


Fig. 9 Pumping power is given for all investigated cases with respect to variation of φ at **a** $Re=500$, **b** $Re=1000$, **c** $Re=1500$, and **d** $Re=2000$. Increasing Re leads to a remarkable increase in pressure drop, hence, in pumping power. Addition of nanoparticles noticeably

decreases the required pumping power due to its relative impacts on viscosity and density. Consideration of twisted rib structure instead of untwisted one can decrease pumping power requirement by up to 43.9%

2000, compared to the base case. It is worth noting that the rate of decrease in pumping power increases with increasing Re , which indicates that the twisted ribs are remarkably advantageous for preventing pressure drops in minichannels, especially at high Re . Therefore, this type of twisted geometry, particularly as in Case 10 or 12, can be recommended for the heat sink applications where pressure drop is critical.

A holistic evaluation of the enhancement in the CHTC versus the augmentation in pressure drop in case of using twisted ribs in the considered heat sink is defined by PEC , where the value of the base case is given as 1 for all investigated parameters, as shown in Fig. 10. As seen from the figure, at $Re = 500$, all PEC values of twisted rib-cases are in the range of 0.81 to 0.91 and lower than that of the base case, which means that their overall hydrothermal performance is lower than the base case. When Re is increased one level,

i.e., to $Re = 1000$, only Case 4 exhibit slightly higher PEC values, while Case 8 and 10 show almost the same PEC values as in the base case. However, it is seen that the number of twisted ribs cases yielding higher PEC values than the base case increases as Re increases. As seen from the figure given for $Re = 2000$, almost all cases have higher PEC values compared to the base case, which are between 0.99 and 1.05. Related to the previous discussion, this variation of PEC with respect to Re is observed because the reduction in the pressure drop caused by the twisted ribs is more profound at higher Re , while the cooling performance of the twisted rib-cases are lower at low Re . Hence, it can be deduced from the PEC values giving the idea for the overall hydrothermal performance that the twisted ribs can be beneficial for higher Re . To sum up here, the twisted fins in the minichannels of the heat sink can regulate the fluid flow and reduce pressure

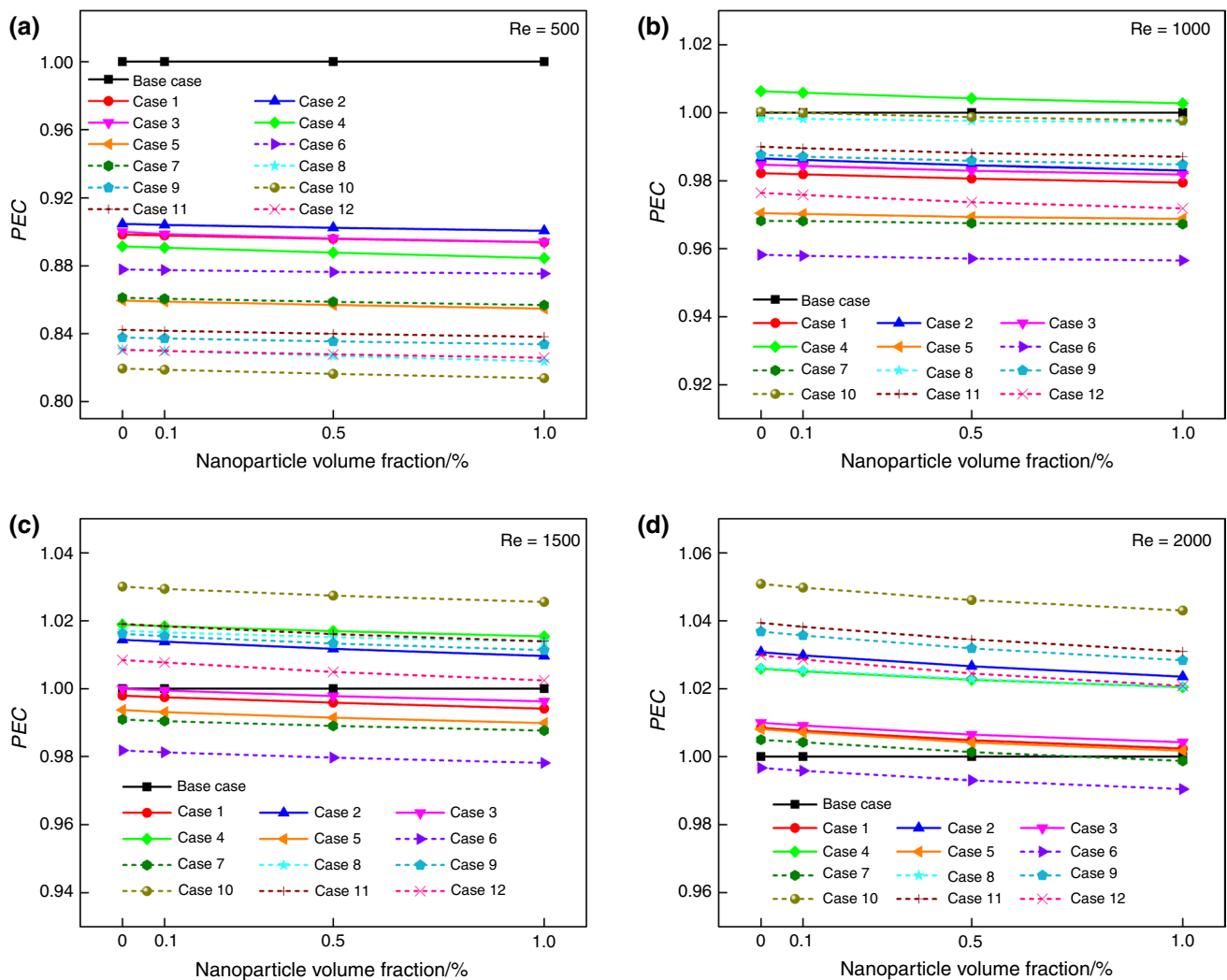


Fig. 10 PEC values are presented for all investigated cases with respect to variation of ϕ at **a** $Re = 500$, **b** $Re = 1000$, **c** $Re = 1500$, and **d** $Re = 2000$. An overall evaluation of hydrothermal performance

shows that the cases having highly twisted ribs, such as Case 10, have a larger PEC values at large Re . At lower Re , e.g., $Re = 500$ and 1000 , the twisted ribs are not advantageous for hydrothermal performance

drop. Nonetheless, as can be seen from the computed *PEC* values, which are useful indicators describing the relative effects of the twisted ribs on the heat transfer and pressure drop holistically in each case, the benefits of using twisted fins are noticeable at relatively higher Reynolds numbers. It is clear that the heat transfer in heat sinks can be enhanced by various methods; however, the pressure drop should not be excessively increased to a level deteriorating overall performance, and it needs to be considered within this scope since it may result in high pumping power requirements. The practical applications where this structure may be possibly used include high heat dissipating electronic devices, high performance computers, and lithium-ion battery packs used for various electric vehicles, where the energy consumption for pumping and heat transfer are both crucial.

The figure of merit (*FoM*) is presented previously to elucidate the impact of nanoparticle addition on the hydrothermal performance inside the minichannels, and the relevant results are shown in Fig. 11. Given its definition, in all examined cases, *FoM* value is unity when the nanoparticle volume fraction is $\varphi = 0\%$, which means the HTF is the pure water. As can be seen from the figure, nanoparticle addition ensures a higher *FoM* in each case, and the values are significantly close to each other. Nevertheless, it is noticed that the *FoM* values are slightly higher in the base case, especially at $Re = 2000$. Quantitatively, at $Re = 2000$, the *FoM* value reaches up to 1.132 in the base case when $\varphi = 1\%$, which indicates that the nanoparticle addition enhances the overall hydrothermal performance in this case by 13.2%. On the other hand, the *FoM* values at this Re are close to

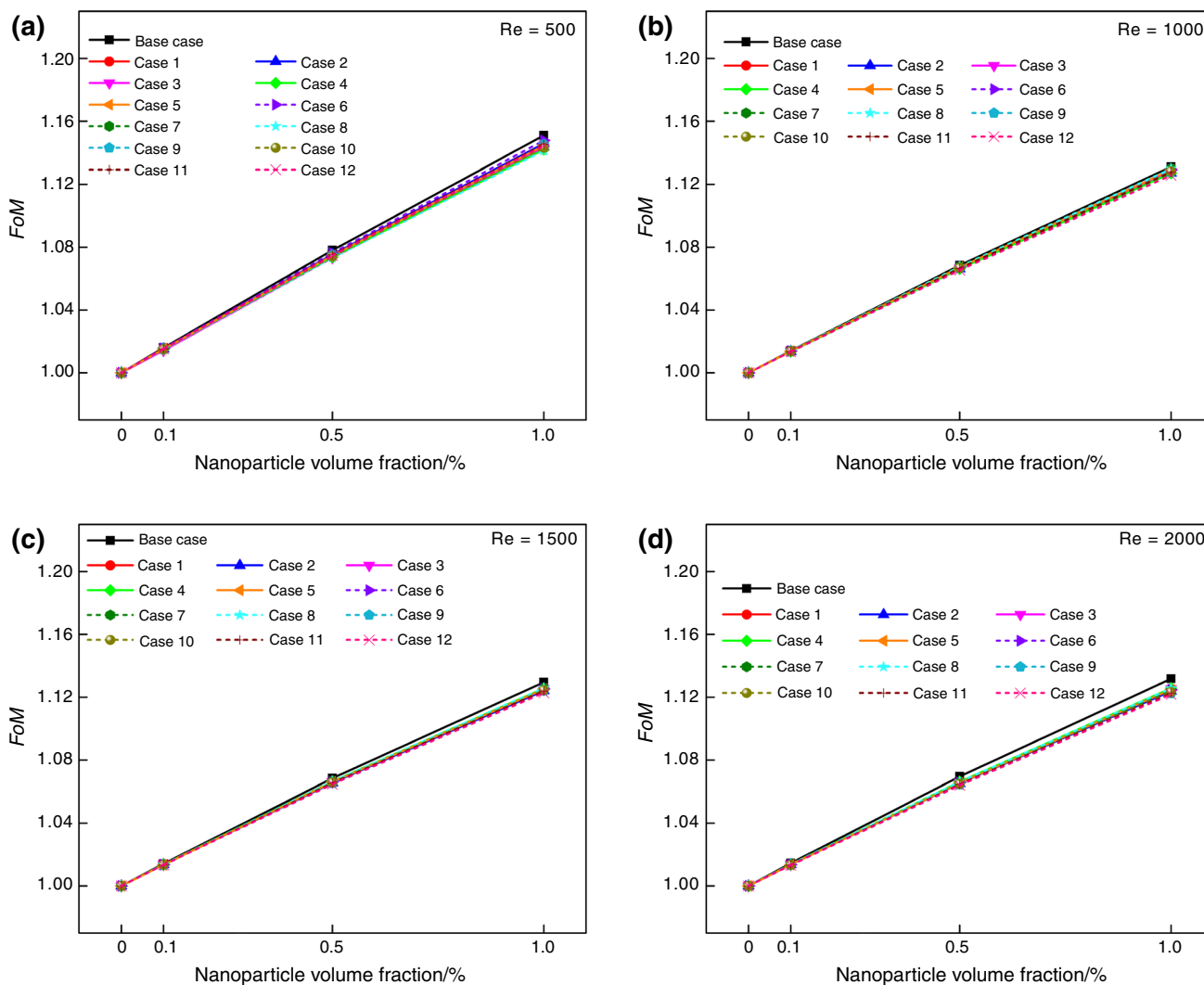


Fig. 11 *FoM* values are depicted here for all investigated cases with respect to variation of φ at **a** $Re = 500$, **b** $Re = 1000$, **c** $Re = 1500$, and **d** $Re = 2000$. Regarding the trends and values of *FoM*, addition of nanoparticles has a remarkably beneficial impact on hydrother-

mal performance. In all cases, inclusion of nanoparticles exhibits a significant improvement, and this improvement is around 13% for all examined cases

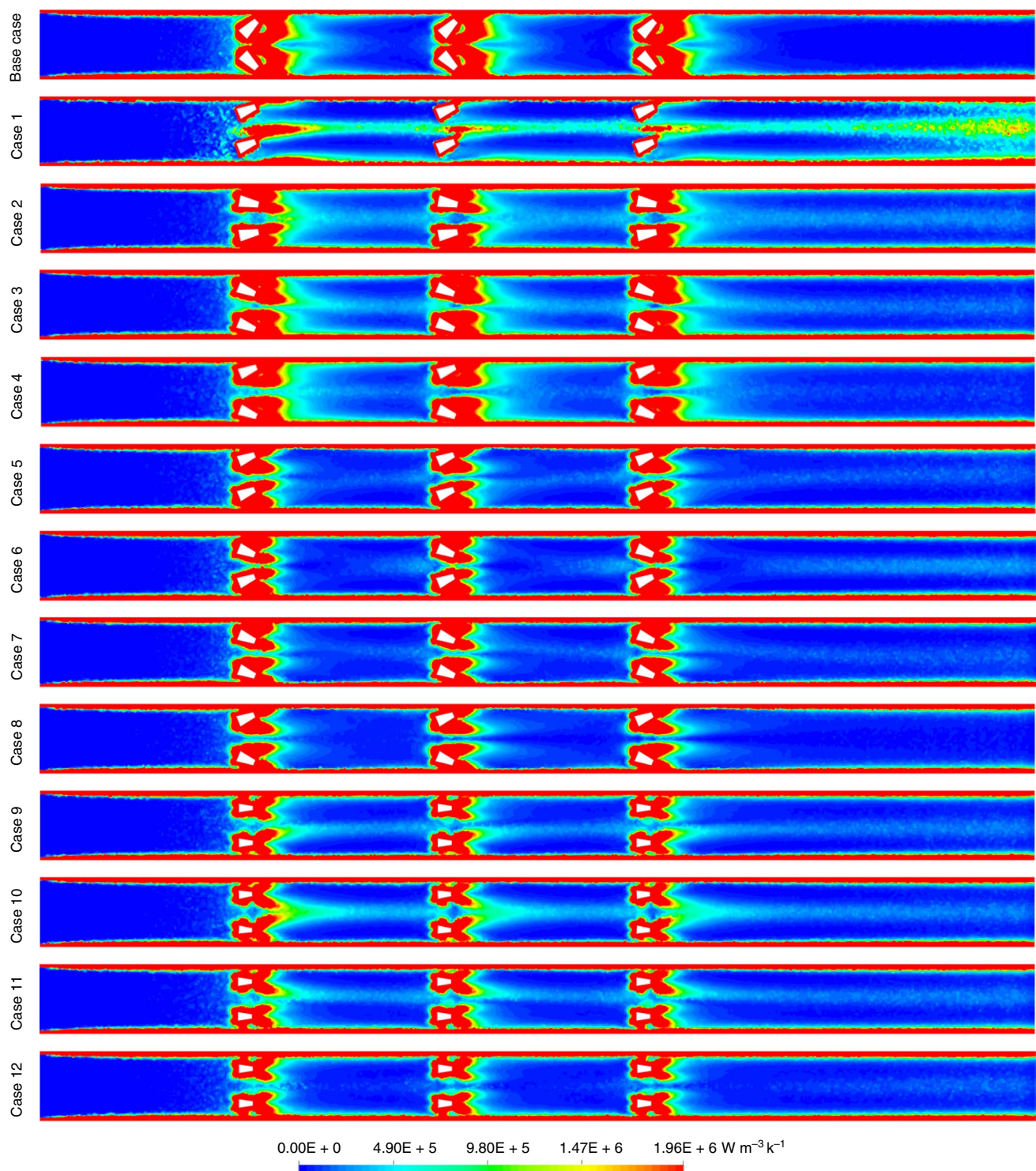


Fig. 12 Local FEG values are illustrated for the investigated cases at $\varphi = 1\%$ and $Re = 2000$ via contours. In the base case, as the ribs are not twisted, the fluid flow is restricted around the ribs, which leads

to a considerable increment of FEG around these areas. On the other hand, the cases with highly twisted ribs, such as Cases 10, 11, and 12, exhibit a smoother flow around the twisted ribs and yield lower FEG

each other and in the range of 1.122 to 1.126, meaning that nanoparticle addition attains an enhancement between 12.2% and 12.6% in case of twisted rib utilization. The reason for

this slight reduction in the twisted cases is that the pressure drop is significantly lower compared to the base case even though the heat transfer performance is also lower. Hence,

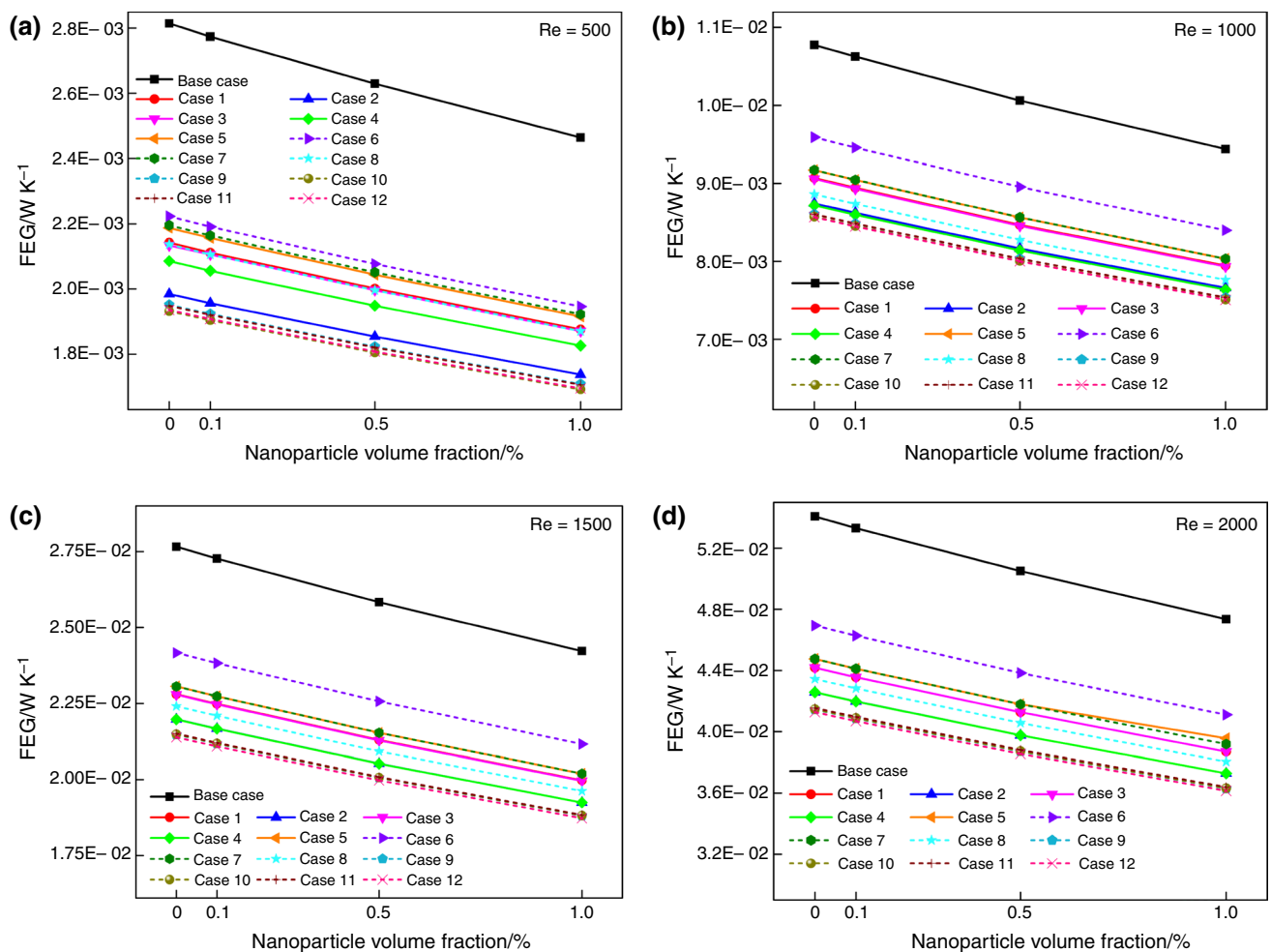


Fig. 13 Global FEG values are given for the investigated cases regarding the variation of φ at **a** $Re=500$, **b** $Re=1000$ **c** $Re=1500$ and **d** $Re=2000$, and it is evidently seen that increasing Re increases

flow intensity, resulting in higher global FEG. As the ribs are not twisted in the base case, the FEG is higher. Adding nanoparticles helps reducing FEG at a certain rate in all investigated cases

the reduction in the heat transfer performance is compensated by the low pressure drop, as a result, the FoM values of the twisted rib-cases were found to be close to the base case with a slight decrease.

Entropy generation characteristics

In this subsection of the paper, the performance of this heat sink geometry, i.e., the twisted ribs geometry is elucidated as per the second law of thermodynamics. Thus, EG characteristics are evaluated by considering the total EG in two branches, namely the frictional and thermal entropy generation, abbreviated by FEG and TEG, respectively.

FEG contours, which display the local variations in the FEG, are shown in Fig. 12 for all the considered cases at $Re=2000$ and $\varphi=1\%$. The regions where the FEG is intense are evidently detected from the figure, and these regions are near the ribs and near the lateral walls of the mini-channel.

This is because the FEG is directly related to the friction factor and pressure drop of a fluid, and thus, FEG is higher in the regions where the fluid flow is restricted, and the viscous forces are dominant. In the base case, where the ribs are not twisted and the nanofluid sharply interacts with the solid surfaces, the FEG active zones are significantly large. Furthermore, even after passing around the ribs, the FEG is partially large in the mini-channel because of the nanofluid has vortices and complicated flow structure which causes considerable augmentation in FEG. On the other hand, twisted rib utilization significantly reduces the high FEG active zones inside the mini-channel as seen from the figure. In particular, the cases with large twist angles at the bottom and top of the ribs, such as Case 11 and 12, exhibit significantly lower FEG around the ribs as well as downstream of the flow since the nanofluid can easily pass between the ribs without any complicity. In addition to these two cases, Case 1 is seen to have remarkably low FEG around the twisted

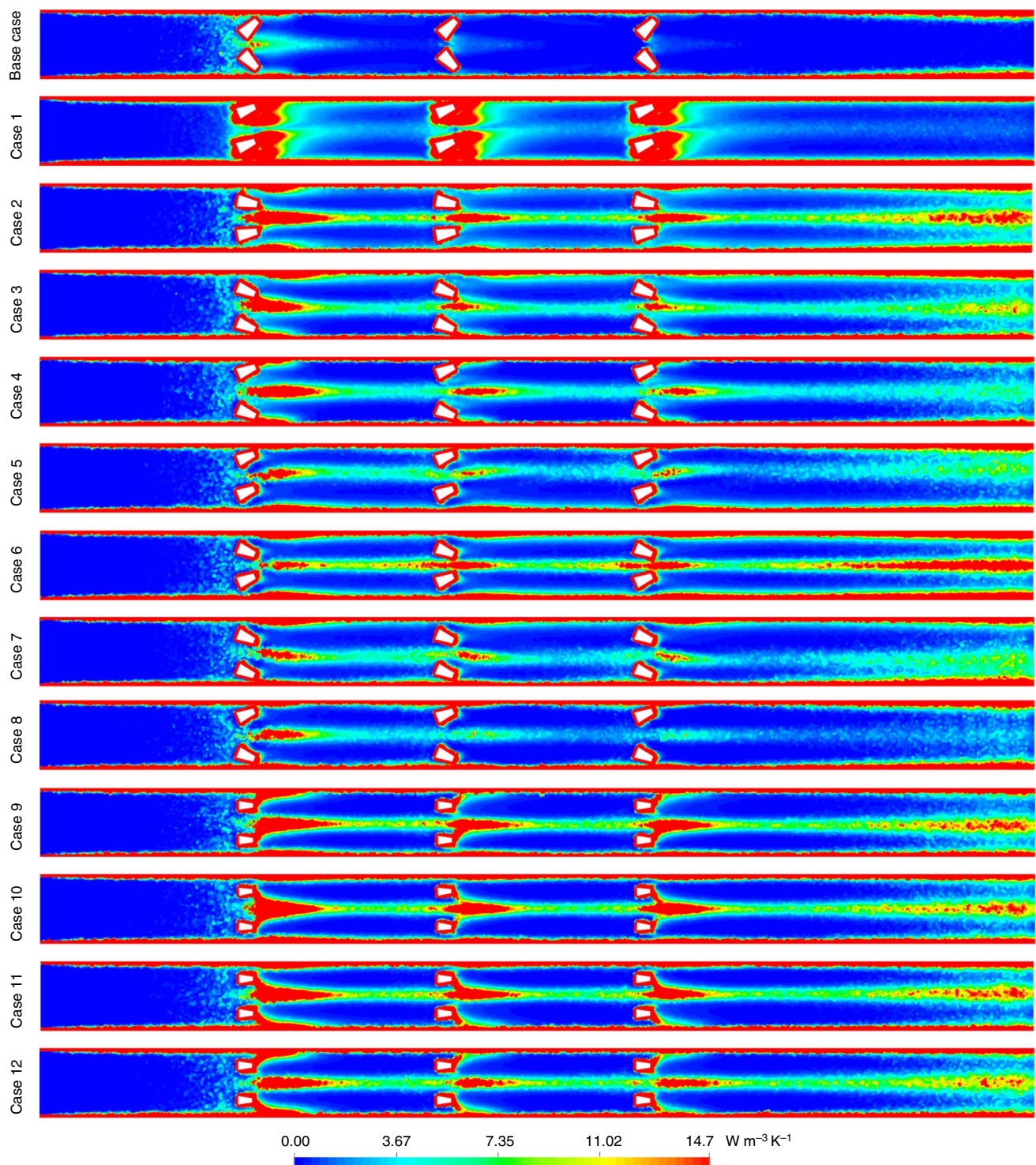


Fig. 14 Local TEG values are illustrated by contours for the investigated cases regarding the variation of φ at **a** $Re=500$, **b** $Re=1000$, **c** $Re=1500$ and **d** $Re=2000$. As a more effective heat transfer is attained in the base case having no twisted ribs, the local TEG val-

ues in this case are noticeably lower. Nonetheless, the flow restriction is low around the twisted ribs, especially in Cases 1, 2, 4, 10, and 12, and this leads to an ineffective heat transfer around these regions, hence, the local TEG becomes higher

ribs. Nevertheless, due to its rib geometry, the nanofluid flow becomes relatively more chaotic through the downstream although it smoothly passes around the twisted ribs. Hence,

from an overall perspective, its FEG value is considered to be higher.

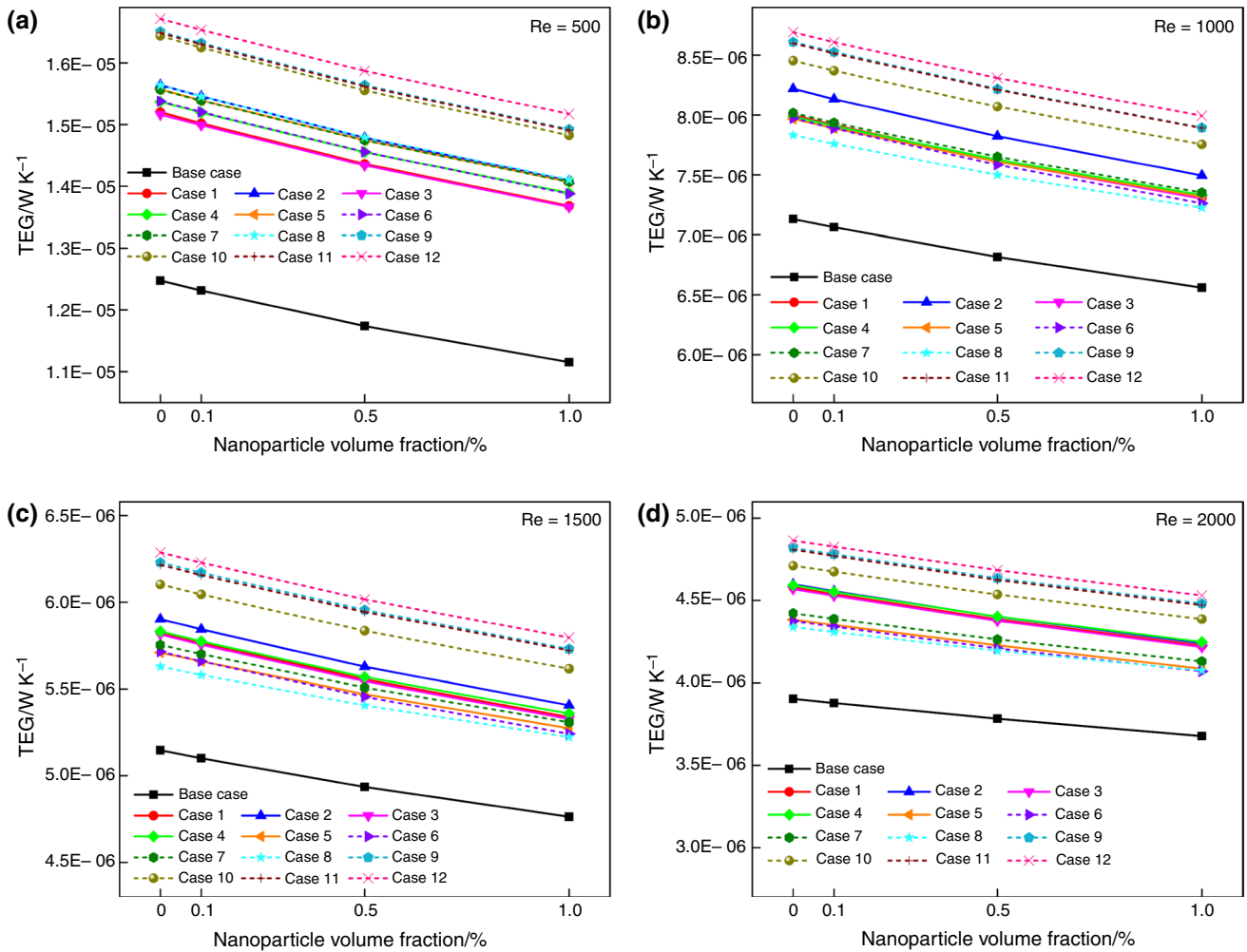


Fig. 15 Global TEG values are given for the investigated cases regarding the variation of φ at **a** $Re=500$, **b** $Re=1000$, **c** $Re=1500$ and **d** $Re=2000$. As Re is increased, TEG decreases due to larger heat transfer and more effective cooling. In the base case, TEG is the

lowest because of high cooling capabilities, while TEG is larger in the cases having twisted ribs especially from top and bottom. Incorporation of nanoparticles improves heat transfer performance and reduces TEG

The global FEG values obtained by the integration of the local values over volume are shown in Fig. 13. In parallel with the interpretations made for the local values, it is observed that the FEGs are significantly higher in the base case, compared to the cases using twisted ribs. The more flow restriction means the larger global FEG, due to the previously mentioned reasons. Selecting Case 4, and Case 12 for a quantitative comparison to the base case at $\varphi = 1\%$, it was found that the FEG is respectively 26% and 31% lower in Case 4 and Case 12, at $Re = 500$, while these reduction rates are 21% and 24% at $Re = 2000$. Considering the impact of nanoparticle addition on reduction of FEG, the numerical results revealed that incorporating nanoparticles into the base fluid has a remarkable reduction effect on FEG. Moreover, it was found that the reduction rate is independent from the fin geometry (i.e., the cases) and Re , which can be noticed from the slope of the line graphs. For instance, in the

base case, Case 4, and Case 12, inclusion of nanoparticles at a concentration of $\varphi = 0.1\%$, 0.5% , and 1% reduces the FEG by 1.4%, 6.6%, and 12.4%, respectively. This is explained by the fact that increasing nanoparticle concentration increases density of the nanofluid, and even though the viscosity also shows an increase, the pressure drop decreases due to larger increment in density relative to viscosity, given a fixed Re .

Figure 14 shows the contours illustrating the local variations of TEG inside the ribbed mini-channel heat sink at $Re = 2000$ and $\varphi = 1\%$. Since the heat transfer in the base case is significantly more intense compared to twisted rib cases, as discussed in Section “Hydrothermal performance”, the TEG active zones are considerably smaller in the base case, compared to the cases with twisted ribs. Particularly in Case 1, Case 2, Case 4, Case 10, and Case 12, TEG is remarkably large because of high irreversibility rate due to their rib geometry reducing heat transfer performance.

Besides, the TEG active zones are significantly more intensified around the ribs, between the ribs, and along the stream of the nanofluid near the outlet, i.e., approximately the last $\frac{1}{4}$ portion of the mini-channel. The reasons for these high TEG locations are first that the nanofluid has significantly low-velocity as they directly contact to the frontal area of the ribs, and thus, the convective currents are significantly weakened in this region. Secondly, the nanofluid directly passing through the twisted ribs without any restriction cannot provide any vortices that can boost the heat transfer; hence, it cannot use its heat rejection potential through the centerline region of the mini-channel. Last but not least, the nanofluid near the outlet section has larger thermal entropy generation because it flows through outlet without sufficient heat rejection, meaning that it cannot use its cooling potential regarding the second law of thermodynamics.

Variation of global TEG is shown in Fig. 15. From the first sight to the y-axes of the graphs, it is deduced from the figure that higher heat transfer rates result in lower TEG. Besides, TEG in the base case is remarkably lower compared to other 12 cases, where the twisted ribs are utilized. Considering Case 4 and Case 12 at $\varphi = 1\%$ for a comparison that is consistent with the discussion of FEG in previous paragraph, the TEG value in Case 4 and Case 12 is 25% and 36% higher than that in the base case when $Re = 500$, respectively, and it is higher by 15% and 23% when Re is considered $Re = 2000$. When nanoparticle inclusion is taken into account in the base case, their contribution is also significant. For instance, at $Re = 500$ in the base case, adding nanoparticle at $\varphi = 0.1\%$, 0.5% , and 1% reduces the TEG by 1.3%, 5.9%, and 10.6%, respectively, compared to using pure water. As Re is increased, the effectiveness of nanoparticle addition decreases, and the TEG reduces by 0.6%, 3.1%, and 5.8%, for the same nanoparticle concentration rates, at $Re = 2000$.

Conclusions

In the present numerical work, twelve different cases using twisted rib geometry inside a nanofluid-cooled mini-channel heat sink were investigated. These twelve cases have twisted ribs at various twist angles at the bottom and/or top of the ribs ranging from -45° to 45° , while one reference case was considered with untwisted ribs for comparisons. Four different Reynolds numbers ($Re = 500$ to 2000) and four different nanoparticle concentrations are taken into account ($\varphi = 0\%$ to 1%) to evaluate the hydrothermal performance and entropy generation inside the minichannels of the heat sink.

It was concluded from the present work that the flow characteristics are significantly affected by the twisted rib

geometry, and the alteration in the flow structure directly affect the convective heat transfer as well as entropy generation behavior of the Ag/water inside the heat sink channel. Moreover, it was found that twisting the ribs both from the top and from the bottom sections, e.g., in Case 10 and 12, makes the flow around the ribs remarkably smoother, compared to the reference case. This situation leads to an easier passage of the fluid; hence, it results in a noticeable decrease in CHTC up to 15.8% (Case 12) at $Re = 2000$ and $\varphi = 1\%$. On the other hand, this phenomenon brings an advantage of lower pumping power requirement by up to 43.9%. Apart from the twisted rib effect, addition of nanoparticles has a significant contribution to the CHTC enhancement, which is more noticeable at low Reynolds numbers. The contribution is slightly higher in the base case, which can reach up to 13.5% in the base case at $\varphi = 1\%$ and $Re = 500$, in comparison to using pure water.

Twisted ribs in the heat sink minichannels play a significant role in entropy generation characteristic as well, due to the fact that twisted ribs have a notable ability to alter the fluid flow. Because of this fluid pattern variations sourced by twisted rib geometry, the pressure drop decreases; thus, frictional entropy generation can be reduced by around 21% to 31% depending on the twist angles and Re . Furthermore, adding nanoparticles at $\varphi = 1\%$ ensures a reduction of 12.4% in the FEG, regardless of considered twisted angle case and Re . On the other hand, using highly twisted ribs as in Case 12 can cause an increase in TEG by 36% and 23%, compared to the base case, at $Re = 500$ and 2000 , respectively, when $\varphi = 1\%$. Addition of nanoparticles is beneficial to decrease TEG, which can reach up to 10.6% in the base case.

Considering the conclusions drawn from the outcomes of this work, the heat sinks with twisted angle ribs can be recommended for the applications, where pressure drop and frictional entropy generation are critical parameters. Nevertheless, it should be noted that using twisted ribs may decrease the cooling performance to some level; hence, this should be taken into account in the practical applications, and the priority of heat transfer enhancement and pressure drop should be determined. Alternatively, various optimization methods can be employed to specify an optimum twisted rib geometry fulfilling the needs and expectations in the considered heat sink application.

Author contributions Amin Shahsavari involved in conceptualization, methodology, software, validation, formal analysis, investigation, writing—review and editing, supervision. Mahan Hasani involved in methodology, software, validation, formal analysis, investigation, writing—original draft, writing—review and editing, visualization. Çağatay Yıldız involved in methodology, software, formal analysis, investigation, writing—original draft, writing—review and editing, visualization. Müslüm Arıcı involved in methodology, formal analysis, investigation, writing—review and editing, supervision.

Funding Open access funding provided by the Scientific and Technological Research Council of Türkiye (TÜBİTAK).

Open Access This article is licensed under a Creative Commons Attribution 4.0 International License, which permits use, sharing, adaptation, distribution and reproduction in any medium or format, as long as you give appropriate credit to the original author(s) and the source, provide a link to the Creative Commons licence, and indicate if changes were made. The images or other third party material in this article are included in the article's Creative Commons licence, unless indicated otherwise in a credit line to the material. If material is not included in the article's Creative Commons licence and your intended use is not permitted by statutory regulation or exceeds the permitted use, you will need to obtain permission directly from the copyright holder. To view a copy of this licence, visit <http://creativecommons.org/licenses/by/4.0/>.

References

- Alhusseny A, Al-Fatlawi A, Al-Aabidy Q, Nasser A, Al-Zurfi N. Dissipating the heat generated in high-performance electronics using graphitic foam heat-sinks cooled with a dielectric liquid. *Int Commun Heat Mass Transf.* 2021;127: 105478. <https://doi.org/10.1016/j.icheatmasstransfer.2021.105478>.
- Wang S, Xing Y, Hao Z, Yin J, Hou X, Wang Z. Experimental study on the thermal performance of PCMs based heat sink using higher alcohol/graphite foam. *Appl Therm Eng.* 2021;198: 117452. <https://doi.org/10.1016/j.applthermaleng.2021.117452>.
- Ho CJ, Hsieh YJ, Rashidi S, Orooji Y, Yan WM. Thermal-hydraulic analysis for alumina/water nanofluid inside a mini-channel heat sink with latent heat cooling ceiling-An experimental study. *Int Commun Heat Mass Transf.* 2020. <https://doi.org/10.1016/j.icheatmasstransfer.2020.104477>.
- Purusothaman A. Investigation of natural convection heat transfer performance of the QFN-PCB electronic module by using nanofluid for power electronics cooling applications. *Adv Powder Technol.* 2018;29:996–1004. <https://doi.org/10.1016/j.apt.2018.01.018>.
- Kumar S, Kumar A, Darshan Kothiyal A, Singh BM. A review of flow and heat transfer behaviour of nanofluids in micro channel heat sinks. *Therm Sci Eng Prog.* 2018;8:477–93. <https://doi.org/10.1016/j.tsep.2018.10.004>.
- Rasangika AHDK, Nasif MS, Pao W, Al-Waked R. Numerical investigation of the effect of square and sinusoidal waves vibration parameters on heat sink forced convective heat transfer enhancement. *Appl Sci.* 2022. <https://doi.org/10.3390/app12104911>.
- Zhang H, Chen L, Liu Y, Li Y. Experimental study on heat transfer performance of lotus-type porous copper heat sink. *Int J Heat Mass Transf.* 2013;56:172–80. <https://doi.org/10.1016/j.ijheatmasstransfer.2012.08.047>.
- He Z, Yan Y, Zhang Z. Thermal management and temperature uniformity enhancement of electronic devices by micro heat sinks: a review. *Energy.* 2021. <https://doi.org/10.1016/j.energy.2020.119223>.
- Ali AM, Angelino M, Rona A. Numerical analysis on the thermal performance of microchannel heat sinks with Al₂O₃ nanofluid and various fins. *Appl Therm Eng.* 2021;198: 117458. <https://doi.org/10.1016/j.applthermaleng.2021.117458>.
- Khaleduzzaman SS, Mahbulul IM, Sohel MR, Saidur R, Selvaraj J, Ward TA, et al. Experimental analysis of energy and friction factor for titanium dioxide nanofluid in a water block heat sink. *Int J Heat Mass Transf.* 2017;115:77–85. <https://doi.org/10.1016/j.ijheatmasstransfer.2017.08.001>.
- Aglawe KR, Yadav RK, Thool SB. Preparation, applications and challenges of nanofluids in electronic cooling: a systematic review. *Mater Today Proc.* 2021;43:366–72. <https://doi.org/10.1016/j.matpr.2020.11.679>.
- Sakanova A, Yin S, Zhao J, Wu JM, Leong KC. Optimization and comparison of double-layer and double-side micro-channel heat sinks with nanofluid for power electronics cooling. *Appl Therm Eng.* 2014;65:124–34. <https://doi.org/10.1016/j.applthermaleng.2014.01.005>.
- Yang L, Du K. Numerical simulation of nanofluid flow and heat transfer in a microchannel: The effect of changing the injection layout arrangement. *Int J Mech Sci.* 2020;172: 105415. <https://doi.org/10.1016/j.ijmecsci.2019.105415>.
- Samudre P, Kailas SV. Thermal performance enhancement in open-pore metal foam and foam-fin heat sinks for electronics cooling. *Appl Therm Eng.* 2022;205: 117885. <https://doi.org/10.1016/j.applthermaleng.2021.117885>.
- Tikadar A, Kumar S. Local hotspot thermal management using metal foam integrated heat sink. *Appl Therm Eng.* 2023;221: 119632. <https://doi.org/10.1016/j.applthermaleng.2022.119632>.
- Senobar H, Aramesh M, Shabani B. Nanoparticles and metal foams for heat transfer enhancement of phase change materials: A comparative experimental study. *J Energy Storage.* 2020. <https://doi.org/10.1016/j.est.2020.101911>.
- Nedumaran MS, Gnanasekaran N, Hooman K. Extensive analysis of PCM-based heat sink with different fin arrangements under varying load conditions and variable aspect ratio. *J Energy Storage.* 2023;73: 108870. <https://doi.org/10.1016/j.est.2023.108870>.
- Yan W, Ye W, Li C. Effect of aspect ratio on saturated boiling flow in microchannels with nonuniform heat flux. *Heat Transf Res.* 2019;48:3312–27. <https://doi.org/10.1002/htj.21543>.
- Gilmore N, Timchenko V, Menictas C. Open manifold microchannel heat sink for high heat flux electronic cooling with a reduced pressure drop. *Int J Heat Mass Transf.* 2020. <https://doi.org/10.1016/j.ijheatmasstransfer.2020.120395>.
- Kong D, Jung E, Kim Y, Manepalli VV, Rah KJ, Kim HS, et al. An additively manufactured manifold-microchannel heat sink for high-heat flux cooling. *Int J Mech Sci.* 2023;248: 108228. <https://doi.org/10.1016/j.ijmecsci.2023.108228>.
- Thakur AK, Prabakaran R, Elkadeem MR, Sharshir SW, Arıcı M, Wang C, et al. A state of art review and future viewpoint on advance cooling techniques for Lithium-ion battery system of electric vehicles. *J Energy Storage.* 2020. <https://doi.org/10.1016/j.est.2020.101771>.
- Li X-J, Zhang J-Z, Tan X-M, Zhang Q-C, Lu E-H. Investigation of fluid flow and heat transfer in a narrow channel with micro barchan-dune-shaped humps. *Int J Mech Sci.* 2022;231: 107589. <https://doi.org/10.1016/j.ijmecsci.2022.107589>.
- Moita A, Moreira A, Pereira J. Nanofluids for the next generation thermal management of electronics: a review. *Symmetry (Basel).* 2021. <https://doi.org/10.3390/sym13081362>.
- Shahsavari A, Ghazizade-Ahsaei H, Baniasad Askari I, Setareh M. Numerical feasibility study of using ultrasonic surface vibration as a new technique for thermal management of the electronic devices. *Energy Convers Manag.* 2023;276: 116481. <https://doi.org/10.1016/j.enconman.2022.116481>.
- Wang Q, Zhang S, Zhang Y, Fu J, Liu Z. Enhancing performance of nanofluid mini-channel heat sinks through machine learning and multi-objective optimization of operating parameters. *Int J Heat Mass Transf.* 2023;210: 124204. <https://doi.org/10.1016/j.ijheatmasstransfer.2023.124204>.
- Yasir M, Khan M, Alqahtani AS, Malik MY. Numerical study of axisymmetric hybrid nanofluid MgO-Ag/H₂O flow with non-uniform heat source/sink. *Alexandria Eng J.* 2023;75:439–46. <https://doi.org/10.1016/j.aej.2023.05.062>.

27. Sriharan G, Harikrishnan S, Oztop HF. A review on thermophysical properties, preparation, and heat transfer enhancement of conventional and hybrid nanofluids utilized in micro and mini channel heat sink. *Sustain Energy Technol Assessments*. 2023;58: 103327. <https://doi.org/10.1016/j.seta.2023.103327>.
28. Ho CJ, Peng J-K, Yang T-F, Rashidi S, Yan W-M. On the assessment of the thermal performance of microchannel heat sink with nanofluid. *Int J Heat Mass Transf*. 2023;201: 123572. <https://doi.org/10.1016/j.ijheatmasstransfer.2022.123572>.
29. Nada SA, El-Zoheiry RM, Elsharnoby M, Osman OS. Enhancing the thermal performance of different flow configuration minichannel heat sink using Al_2O_3 and CuO-water nanofluids for electronic cooling: an experimental assessment. *Int J Therm Sci*. 2022;181: 107767. <https://doi.org/10.1016/j.ijthermalsci.2022.107767>.
30. Boudraa B, Bessaïh R. Three-dimensional analysis of heat transfer and entropy production of jet impingement hybrid nanofluid cooling a porous media-filled heat sink. *Energy Sourc Part A Recover Util Environ Eff*. 2022;44:6035–62. <https://doi.org/10.1080/15567036.2022.2095460>.
31. Marseglia G, De Giorgi MG, Pontes P, Solipa R, Souza RR, Moreira ALN, et al. Enhancement of microchannel heat sink heat transfer: Comparison between different heat transfer enhancement strategies. *Exp Therm Fluid Sci*. 2024;150: 111052. <https://doi.org/10.1016/j.expthermflusc.2023.111052>.
32. Ma Z, Hu C, Ma L, Chen H, Hou J, Hao N, et al. Nanofluids in microchannel heat sinks for efficient flow cooling of power electronic devices. *Appl Mater Today*. 2023;35: 101980. <https://doi.org/10.1016/j.apmt.2023.101980>.
33. Mukherjee S, Wciślik S, Khadanga V, Mishra PC. Influence of nanofluids on the thermal performance and entropy generation of varied geometry microchannel heat sink. *Case Stud Therm Eng*. 2023;49: 103241. <https://doi.org/10.1016/j.csite.2023.103241>.
34. Ho CJ, Peng J-K, Yang T-F, Rashidi S, Yan W-M. Comparison of cooling performance of nanofluid flows in mini/micro-channel stacked double-layer heat sink and single-layer micro-channel heat sink. *Int J Therm Sci*. 2023;191: 108375. <https://doi.org/10.1016/j.ijthermalsci.2023.108375>.
35. Yan W, Li C, Ye W. Numerical investigation of hydrodynamic and heat transfer performances of nanofluids in a fractal microchannel heat sink. *Heat Transf Res*. 2019;48:2329–49. <https://doi.org/10.1002/htj.21494>.
36. Mozafari M, Lee A, Mohammadpour J. Thermal management of single and multiple PCMs based heat sinks for electronics cooling. *Therm Sci Eng Prog*. 2021. <https://doi.org/10.1016/j.tsep.2021.100919>.
37. Zahid I, Farhan M, Farooq M, Asim M, Imran M. Experimental investigation for thermal performance enhancement of various heat sinks using Al_2O_3 NePCM for cooling of electronic devices. *Case Stud Therm Eng*. 2023;41: 102553. <https://doi.org/10.1016/j.csite.2022.102553>.
38. Horiuchi K, Nishihara A, Sugimura K. Multi-objective optimization of water-cooled pinfin heatsinks. *Int J Heat Mass Transf*. 2015;81:760–6. <https://doi.org/10.1016/j.ijheatmasstransfer.2014.10.057>.
39. Chiam ZL, Lee PS, Singh PK, Mou N. Investigation of fluid flow and heat transfer in wavy micro-channels with alternating secondary branches. *Int J Heat Mass Transf*. 2016;101:1316–30. <https://doi.org/10.1016/j.ijheatmasstransfer.2016.05.097>.
40. Sheremet MA, Rashidi MM. Thermal convection of nano-liquid in an electronic cabinet with finned heat sink and heat generating element. *Alexandria Eng J*. 2021;60:2769–78. <https://doi.org/10.1016/j.aej.2021.01.013>.
41. Yan Y, Zhao T, He Z, Yang Z, Zhang L. Numerical investigation on the characteristics of flow and heat transfer enhancement by micro pin-fin array heat sink with fin-shaped strips. *Chem Eng Process - Process Intensif*. 2021;160: 108273. <https://doi.org/10.1016/j.ccep.2020.108273>.
42. Azadi M, Hosseini-rad E, Hormozi F, Rashidi S. Second law analysis for nanofluid flow in mini-channel heat sink with finned surface: a study on fin geometries. *J Therm Anal Calorim*. 2020;140:1883–95. <https://doi.org/10.1007/s10973-019-08921-2>.
43. Khetib Y, Sedraoui K, Melaibari AA, Alzaied A, Alsulami R, Sharifpur M. Heat transfer and pressure drop in turbulent nanofluid flow in a pin-fin heat sink: Fin and nanoparticles shape effects. *Case Stud Therm Eng*. 2021;28: 101378. <https://doi.org/10.1016/j.csite.2021.101378>.
44. Nawaz S, Babar H, Ali HM, Sajid MU, Janjua MM, Said Z, et al. Oriented square shaped pin-fin heat sink: performance evaluation employing mixture based on ethylene glycol/water graphene oxide nanofluid. *Appl Therm Eng*. 2022. <https://doi.org/10.1016/j.applthermaleng.2022.118085>.
45. Babar H, Wu H, Ali HM, Shah TR, Zhang W. Staggered oriented airfoil shaped pin-fin heat sink: investigating the efficacy of novel water based ferric oxide-silica hybrid nanofluid. *Int J Heat Mass Transf*. 2022. <https://doi.org/10.1016/j.ijheatmasstransfer.2022.123085>.
46. Zheng S, Feng Z, Lin Q, Hu Z, Lan Y, Guo F, et al. Numerical investigation on thermal-hydraulic characteristics in a mini-channel with trapezoidal cross-section longitudinal vortex generators. *Appl Therm Eng*. 2022. <https://doi.org/10.1016/j.applthermaleng.2021.118004>.
47. Wang H, Chen X. Performance improvements of microchannel heat sink using Koch fractal structure and nanofluids. *Structures*. 2023;50:1222–31. <https://doi.org/10.1016/j.istruc.2023.02.109>.
48. Li C, Li X, Huang H, Zheng Y. Hydrothermal performance analysis of microchannel heat sink with embedded module with ribs and pin-fins. *Appl Therm Eng*. 2023;225: 120167. <https://doi.org/10.1016/j.applthermaleng.2023.120167>.
49. Zhang JF, Jia L, Yang WW, Taler J, Oclon P. Numerical analysis and parametric optimization on flow and heat transfer of a microchannel with longitudinal vortex generators. *Int J Therm Sci*. 2019;141:211–21. <https://doi.org/10.1016/j.ijthermalsci.2019.03.036>.
50. Zhang Q, Feng Z, Li Z, Chen Z, Huang S, Zhang J, et al. Numerical investigation on hydraulic and thermal performances of a mini-channel heat sink with twisted ribs. *Int J Therm Sci*. 2022. <https://doi.org/10.1016/j.ijthermalsci.2022.107718>.
51. Chang SW, Kang CH, Lee CL, Yu CH. Effect of pitching and rolling motion on hydrothermal performance of rectangular channel flow enhanced by twisted-tape pin-fin array. *Appl Therm Eng*. 2021. <https://doi.org/10.1016/j.applthermaleng.2021.116971>.
52. Chang SW, Wu PS, Cai WL, Yu CH. Experimental heat transfer and flow simulations of rectangular channel with twisted-tape pin-fin array. *Int J Heat Mass Transf*. 2021. <https://doi.org/10.1016/j.ijheatmasstransfer.2020.120809>.
53. Shahsavari A, Entezari S, Askari IB, Ali HM. The effect of using connecting holes on heat transfer and entropy generation behaviors in a micro channels heat sink cooled with biological silver/water nanofluid. *Int Commun Heat Mass Transf*. 2021. <https://doi.org/10.1016/j.icheatmasstransfer.2020.104929>.
54. Huaxu L, Fuqiang W, Dong Z, Ziming C, Chuanxin Z, Bo L, et al. Experimental investigation of cost-effective ZnO nanofluid based spectral splitting CPV/T system. *Energy*. 2020;194: 116913. <https://doi.org/10.1016/j.energy.2020.116913>.
55. Shahsavari A, Heidarian M, Yıldız Ç, Arıcı M. Effect of opening pin fin arrangement on the thermal performance and entropy generation of a heat sink cooled by biologically synthesized silver-water nanofluid. *Eng Anal Bound Elem*. 2023;150:599–611. <https://doi.org/10.1016/j.enganabound.2023.02.033>.

56. Imran AA, Mahmoud NS, Jaffal HM. Numerical and experimental investigation of heat transfer in liquid cooling serpentine mini-channel heat sink with different new configuration models. *Therm Sci Eng Prog.* 2018;6:128–39. <https://doi.org/10.1016/j.tsep.2018.03.011>.
57. Ambreen T, Saleem A, Park CW. Numerical analysis of the heat transfer and fluid flow characteristics of a nanofluid-cooled micro-pin-fin heat sink using the Eulerian–Lagrangian approach. *Powder Technol.* 2019;345:509–20. <https://doi.org/10.1016/j.powtec.2019.01.042>.
58. Vahabzadeh Bozorg M, Siavashi M. Two-phase mixed convection heat transfer and entropy generation analysis of a non-Newtonian nanofluid inside a cavity with internal rotating heater and cooler. *Int J Mech Sci.* 2019;151:842–57. <https://doi.org/10.1016/j.ijmecsci.2018.12.036>.
59. Shahsavar A, Baseri MM, Al-Rashed AAAA, Afrand M. Numerical investigation of forced convection heat transfer and flow irreversibility in a novel heatsink with helical microchannels working with biologically synthesized water-silver nano-fluid. *Int Commun Heat Mass Transf.* 2019. <https://doi.org/10.1016/j.icheatmasstransfer.2019.104324>.
60. Yao P, Zhai Y, Ma M, Li Y, Wang H. An improving performance evaluation plot (PEP) for energy management in microchannel heat sinks by using nanofluids. *Int Commun Heat Mass Transf.* 2020. <https://doi.org/10.1016/j.icheatmasstransfer.2020.104808>.
61. Shahsavar A, Farhadi P, Yıldız Ç, Moradi M, Arici M. Evaluation of entropy generation characteristics of boehmite-alumina nanofluid with different shapes of nanoparticles in a helical heat sink. *Int J Mech Sci.* 2022. <https://doi.org/10.1016/j.ijmecsci.2022.107338>.
62. Hazeri-Mahmel N, Shekari Y, Tayebi A. Three-dimensional analysis of forced convection of Newtonian and non-Newtonian nanofluids through a horizontal pipe using single- and two-phase models. *Int Commun Heat Mass Transf.* 2021;121: 105119. <https://doi.org/10.1016/j.icheatmasstransfer.2021.105119>.
63. Garoosi F, Rashidi MM. Two phase flow simulation of conjugate natural convection of the nanofluid in a partitioned heat exchanger containing several conducting obstacles. *Int J Mech Sci.* 2017;130:282–306. <https://doi.org/10.1016/j.ijmecsci.2017.06.020>.
64. Hasani M, Baniasad Askari I, Shahsavar A. Two-phase mixture simulation of the performance of a grooved helical microchannel heat sink filled with biologically prepared water-silver nanofluid: hydrothermal characteristics and irreversibility behavior. *Appl Therm Eng.* 2022;202: 117848. <https://doi.org/10.1016/j.applthermaleng.2021.117848>.
65. Bakhti FZ, Si-Ameur M. A comparison of mixed convective heat transfer performance of nanofluids cooled heat sink with circular perforated pin fin. *Appl Therm Eng.* 2019. <https://doi.org/10.1016/j.applthermaleng.2019.113819>.
66. Khoshvaght-Aliabadi M, Deldar S, Hassani SM. Effects of pin-fins geometry and nanofluid on the performance of a pin-fin miniature heat sink (PFMHS). *Int J Mech Sci.* 2018;148:442–58. <https://doi.org/10.1016/j.ijmecsci.2018.09.019>.
67. Shahsavar A, Shahmohammadi M, Askari IB. CFD simulation of the impact of tip clearance on the hydrothermal performance and entropy generation of a water-cooled pin-fin heat sink. *Int Commun Heat Mass Transf.* 2021;126: 105400. <https://doi.org/10.1016/j.icheatmasstransfer.2021.105400>.
68. Yang L, Du K, Zhang Z. Heat transfer and flow optimization of a novel sinusoidal minitube filled with non-Newtonian SiC/EG-water nanofluids. *Int J Mech Sci.* 2020;168: 105310. <https://doi.org/10.1016/j.ijmecsci.2019.105310>.
69. Jitheesh EV, Joseph M, Sajith V. Comparison of metal oxide and composite phase change material based nanofluids as coolants in mini channel heat sink. *Int Commun Heat Mass Transf.* 2021;127: 105541. <https://doi.org/10.1016/j.icheatmasstransfer.2021.105541>.
70. Lori MS, Vafai K. Heat transfer and fluid flow analysis of micro-channel heat sinks with periodic vertical porous ribs. *Appl Therm Eng.* 2022;205: 118059. <https://doi.org/10.1016/j.applthermaleng.2022.118059>.
71. Yıldız Ç, Yıldız AE, Arıcı M, Azmi NA, Shahsavar A. Influence of dome shape on flow structure, natural convection and entropy generation in enclosures at different inclinations: a comparative study. *Int J Mech Sci.* 2021. <https://doi.org/10.1016/j.ijmecsci.2021.106321>.
72. Ambreen T, Saleem A, Park CW. Analysis of hydro-thermal and entropy generation characteristics of nanofluid in an aluminium foam heat sink by employing Darcy–Forchheimer–Brinkman model coupled with multiphase Eulerian model. *Appl Therm Eng.* 2020. <https://doi.org/10.1016/j.applthermaleng.2020.115231>.
73. Liu C, Teng J, Chu J-C, Chiu Y, Huang S, Jin S, et al. Experimental investigations on liquid flow and heat transfer in rectangular microchannel with longitudinal vortex generators. *Int J Heat Mass Transf.* 2011;54:3069–80. <https://doi.org/10.1016/j.ijheatmasstransfer.2011.02.030>.
74. Hong FJ, Cheng P, Ge H, Joo GT. Conjugate heat transfer in fractal-shaped microchannel network heat sink for integrated microelectronic cooling application. *Int J Heat Mass Transf.* 2007;50:4986–98. <https://doi.org/10.1016/j.ijheatmasstransfer.2007.09.006>.
75. Izadi S, Armaghani T, Ghasemiasl R, Chamkha AJ, Molana M. A comprehensive review on mixed convection of nanofluids in various shapes of enclosures. *Powder Technol.* 2019;343:880–907. <https://doi.org/10.1016/j.powtec.2018.11.006>.

Publisher's Note Springer Nature remains neutral with regard to jurisdictional claims in published maps and institutional affiliations.